

Republic of Iraq  
Ministry of Higher Education and Scientific Research  
AL-Nahrain University  
College of Science



# *A Computational Optimization of Magnetic System Consists of Deflector and Lens*

**A Thesis**

Submitted to the College of Science of Al-Nahrain  
University in Partial Fulfillment of the Requirements  
for the Degree of Master of Science in Physics

**By**

*Ahmad Hussein Ali*

(B.Sc.2006)

Supervised by

*Dr. Ahmad Kamal Ahmad & Dr. Oday Ali Hussein*

In

Thou Al-Hujaa 1429 A. H.

December 2008 A. D.

بِسْمِ اللَّهِ الرَّحْمَنِ الرَّحِيمِ

وَأَنْ لَّيْسَ لِلْإِنْسَانِ إِلَّا مَا سَعَى (39)  
وَأَنْ سَعْيُهُ سَوْفَ يُرَى (40) ثُمَّ يُجْزَاهُ  
الْجِزَاءَ الْأَوْفَى (41)

صدق الله العظيم  
من سورة النجم

# *Certification*

I certify that this thesis entitled “**A Computational Optimization of Magnetic System Consists of Deflector and Lens**” is prepared by *Mr. Ahmad Hussein Ali* under our supervision at the College of Science of Al-Nahrain University in partial fulfillment of the requirements for the degree of **Master of Science in Physics**.

**Supervisor: Dr. Ahmad K. Ahmad**

**Supervisor: Dr. Oday A. Hussein**

**Title: Assistant Professor**

**Title: Lecturer**

**Date: / /2008**

**Date: / /2008**

In view of the recommendations, I present this thesis for debate by the examination committee.

**Dr. Ahmad K. Ahmad**

**Title: Assistant Professor**

**Head of Physics Department**

**Date: / /2008**

**Dedicated to**

**My Family**

# *Acknowledgments*

*First of all, I would like to thank almighty ALLAH for gifting me a spot light, which has given me hope, patience, and a new thinking for a better life.*

*Secondly, I would like to thank the messenger of peace Mohammed, the prophet of humans.*

*I would like to express my sincere thanks and deep appreciation to my supervisors, Dr. Ahmad K, Ahmad and Dr. Oday A. Hussein for suggesting the project of research, helpful discussions and comments throughout this work, and for reading the manuscript of this thesis.*

*A special thank to Mr. Mahdi Ahmad for valuable assistance during the work,*

*I am grateful to the Dean of College of science and the staff of the Department of physics at Al-Nahrain University for their valuable support and cooperation. I thank the staff of the library of Al-Nahrain University. My special thanks to all my friends for encouragement and support during the work,*

*Last but not least, I would like to record my deep affection and thanks to my parent for their moral support and patience throughout this work,*

*Ahmad*

# Contents

<i>Abstract</i> .....	I
<i>List of Symbols</i> .....	III

## Chapter One

### Introduction

<i>1.1 Introduction</i> .....	1
<i>1.2 Magnetic Deflector</i> .....	1
<i>1.3 Types of Magnetic Deflector</i> .....	1
<i>1.4 Magnetic Lenses</i> .....	2
<i>1.5 Type of Magnetic Lenses</i> .....	3
<i>1.6 Properties of Magnetic Lenses</i> .....	3
<i>1.7 Advantage of Magnetic Lenses and Deflectors</i> .....	4
<i>1.8 Historical Review</i> .....	4
<i>1.9 Optimization Method</i> .....	7
<i>1.14 Aim of the theses</i> .....	8

# Chapter Two

## Theoretical Considerations

<i>2.1 Introduction.....</i>	9
<i>2.2 Paraxial-Ray Equation in Magnetic Fields.....</i>	9
<i>2.3 Optical Parameters and Initial Condition.....</i>	10
<i>2.4 Magnetic Deflection Fields.....</i>	12
<i>2.5Magnetic Scalar Potential Calculation.....</i>	13
<i>2.6 Pole Piece Reconsideration.....</i>	15
<i>2.7 The Moving Objective Lens (MOL) Concept.....</i>	15
<i>2.8 Aberrations of Axially Symmetric Electron-Optical Systems.....</i>	17
<i>2.8.1 Spherical aberration.....</i>	17
<i>2.8.2 Chromatic aberration.....</i>	19
<i>2.8.3 Radial and spiral distortions.....</i>	21

# Chapter Three

## Results and Discussion

<i>3.1 The Behavior of the Magnetic Deflector and Lens at Difference Values of Length and Angle of Coil.....</i>	25
<i>3.2 Design Using Exponential Model.....</i>	26
<i>3.3 Electron Beam Trajectory.....</i>	30
<i>3.4 Infinite Magnification Condition.....</i>	33
<i>3.4.1 Effects of changing the length.....</i>	33

<i>a- Relative spherical and chromatic aberration coefficients</i> .....	33
<i>b- Relative radial and spiral distortion coefficients</i> .....	37
3.4.2 <i>Effects of changing the angle</i> .....	40
<i>a- Relative spherical and chromatic aberration coefficient</i> .....	40
<i>b- Relative radial and spiral distortion coefficients</i> .....	43
3.5 <i>Zero Magnification Condition</i> .....	47
3.5.1 <i>Effects of changing the length</i> .....	47
<i>a- Relative spherical and chromatic aberration coefficients</i> .....	47
<i>b- Relative radial and spiral distortion coefficients</i> .....	50
3.5.2 <i>Effects of changing the angle</i> .....	52
<i>a- Relative spherical and chromatic aberration coefficients</i> .....	52
<i>b- Relative radial and spiral distortion coefficients</i> .....	56
3.6 <i>Pole Pieces Reconstruction</i> .....	59

## *Chapter Four*

### Conclusions and Suggestions for Future Work

4.1 <i>Conclusions</i> .....	60
4.2 <i>Recommendations for Future Work</i> .....	61
Reference.....	62



## *Abstract*

A computation investigation on the design of magnetic deflection and focusing system using the synthesis approach of optimization method has been done. By solving the paraxial ray equation using the Runge-Kutta-Nystrom method the trajectories of the electron beam and the optical properties of the magnetic deflection and focusing system under infinite and zero magnification conditions has been computed.

The synthesis approach of optimization method is used in the present work to finding the optimum design of magnetic deflection and focusing system which give rise to the minimum spherical, chromatic, spiral distortion, and radial distortion aberration.

The toroidal deflection coil is used as the source of magnetic field, and then the field distribution is determined by using an exponential function. The moving objective lens concept is included in the computation of system field.

The system aberration has been minimized by changing the geometrical shape of the toroidal coil, where the length and angle of the coil varied. By using the optimum axial field distribution, the pole pieces shape which gives rise to these field distributions is found by using the reconstruction method.

Computation shows that the smaller aberration coefficients occur when the length of the coil ( $H= 23\text{mm}$ ) and angle of the coil ( $\theta=61^\circ$ ). The relationship between the four coefficients and length and angle of the coil is

inverse proportional in the cases of zero and infinite magnification conditions, therefore, provides us with the possibility of operating the system with high efficiency in different operation conditions of the system.

## *List of Symbols*

a	The field width at half maximum $B_m / 2$ .
$B(z)$	Magnetic flux density (Tesla).
$B_m$	Maximum value of axial magnetic flux density distribution (Tesla).
$B_x(z)$	The deflection field at the axis of an air core toroidal yoke (Tesla).
$C_c$	Chromatic aberration coefficient (m).
$C_s$	Spherical aberration coefficient (m).
D	Distortion coefficient (m).
$D(z)$	Deflection magnetic flux density (Tesla).
$D_{rad}$	Radial distortion coefficient (m).
$D_{sp}$	Spiral distortion coefficient (m).
d	Displacement by the first magnetic deflector (m).
$E_0$	Energy of electron beam.
e	Electron charge ( $1.6 \times 10^{-19}$ C).
$F_p$	Projector focal length (mm).
H	The length of the toroidal coil (mm).
h	Solution of paraxial ray equation.
L	The length of the system field.
M	Liner magnification.
m	Electron mass ( $m = 9.1 \times 10^{-31}$ Kg).
NI	Magnetic excitation (Ampere-turns).
$NI / (V_r)^{0.5}$	Magnetic excitation parameter (Ampere-turns/(Volt) <sup>0.5</sup> ).
R	Radial displacement of the beam from the optical axis (m).
$R_p(z)$	Radial height of the pole pieces along the optical axis (m).
r	Distance of the corresponding object point from the axis (m).

$r_s$	Fluctuation in the electron beam focus.
$V_a$	Accelerating voltage (Volt).
$V_p$	Pole piece potential (Volt).
$V_r$	Relativistic corrected accelerating voltage (Volt).
$V_z=V(z)$	Axial magnetic scalar potential (Volt).
X and Y	Two independent solutions of the paraxial-ray equation.
z	Length of the optical axis along the system (m).
$z_i$	Image plane position (m).
$z_o$	Object plane position (m).
$\alpha$	Trajectory angle with system axis (degree).
$\beta$	Angle of the arriving electrons (degree).
$\Delta E_o$	Fluctuation in the electron beam energy.
$\mu_o$	Permeability of free space ( $\mu_o = 4 \pi * 10^{-7} \text{ H.m}^{-1}$ ).
$\varphi$	Angle of the coil (degree).

*Chapter*  
*One*

*Introduction*

**1**

# *Chapter One*

## Introduction

### **1.1 Introduction**

In many electron beam instruments, such as scanning electron microscopes and scanning electron beam lithography systems are usually use a magnetic lens to focus a(charge) particle beam , and magnetic deflection coils mounted with in the lens.

In particular, the relationship between focusing magnetic field of the lens and the deflection field must be optimized for minimum aberration and normal landing angle [**Lencova and Wisselink 2001**].

### **1.2 Magnetic Deflectors**

The magnetic deflectors are used to steer the beam in the desired direction [**Philip Coane 1999**].

The most common and classical type of deflection is used in cathode ray tubes and scanning electron microscopes . Its purpose is to scan the beam over a surface [**Szilagy 1988**].

### **1.3 Types of Magnetic Deflector**

In the magnetic deflectors, two geometries are common

a- Toroidal magnetic deflection system: Systems of this kind are used in television tubes, and in scanning microscopes for deflecting the electron beam. In toroidal structure figure (1-1).Two pairs of coils, rotated at  $90^\circ$

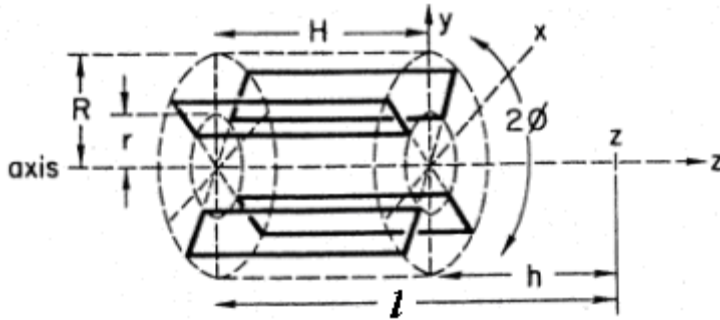


**Figure (1-1) Toroidal deflection coil [Hawkes and Kasper 1989].**

**b-** Saddle coil: saddle coil, shown in figure (1-2) is usually enclosed in a ferrite sheathe, there by reducing the wastage of flux. The shielding is omitted only in devices designed to function at high deflection frequencies in order to decrease the inductance[Hawkes 1989].

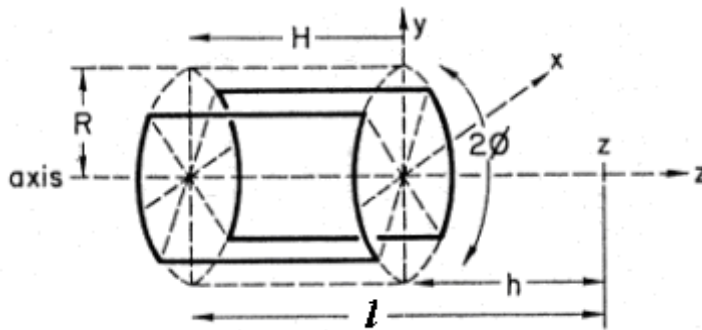


**Figure (1-2) Saddle deflection coil (Hawkes and Kasper 1989).**

## 1.4 Magnetic Lenses

To focus an electron beam, a magnetic lens employs the magnetic field produced by a coil carrying a direct current [Egerton 2007]. Manufacturing

of magnetic lenses is usually more complicated than that of electrostatic lenses.

The magnetic lenses have extensive applications in such areas as electron microscopy and cathode ray tubes [Humphries 1999].

## 1.5 Types of Magnetic Lenses

Magnetic lenses can be classified from various points of view. For example, one can mention **(a)** thick or thin lenses, according to the change in the slope of the trajectory of the beam passing through the lens, **(b)** strong or weak lenses depending on whether their focal points are situated inside or outside the magnetic field, **(c)** symmetric or asymmetric lenses depending upon whether there exists a middle plane perpendicular to the lens axis about which the geometrical arrangement of the lens is symmetric or not, **(d)** doublet or singlet depending on whether the lens has two or one air gap. Furthermore, magnetic lenses may be long or short, iron-free or shrouded by ferromagnetic materials.

Magnetic lenses may be classified according to the number of pole pieces in the lens. According to the criteria magnetic lenses can be classified into four types namely, single pole piece, double pole piece, triple pole piece, and the iron-free [Szilagyı 1988].

## 1.6 Properties of Magnetic Lenses

The lens properties can be determined once the real lens field is replaced by an ideal rectangular field of length  $L$ . Physically this ideal field is that of a solenoid of length  $S$  and diameter  $2/3D$  carrying the same ampere – turns  $NI$  (**excitation**) (i.e. number of turns  $\times$  D.C. current). The diagonal  $L$  of the solenoid is related to the real lens geometry by [Lencova 1997]:



$$L = \sqrt{(S)^2 + (2/3 D)^2} \quad (1-1)$$

The maximum magnetic flux density  $B_{max}$  is given by [**Lencova and Wisselink 2001**]:

$$B_{max} = (\mu_0 \times NI)/L \quad (1-2)$$

where  $L$  is geometrical parameter,  $\mu_0$  is the permeability of free space. Therefore, the magnetic field generated by a magnetic lens depends on its shape and excitation  $NI$ .

The distinctive feature of magnetic lenses is that their optical properties are dependent on the charge to mass ratio of the particles. In magnetic lenses the particle trajectories depend on the particles mass, where heavy particles are less focused than light ones.

Magnetic lenses are used for forming electron optical system which transforms an 'object' into 'image' [**Goodhew et al 2001**].

## **1.7 Advantage of Magnetic Lenses and Deflectors**

Compared with electrostatic lens and deflector, magnetic lens and deflector have some advantages [**Liu 2005**]:

- 1- High stability
- 2- Low aberration
- 3- High sensitivity

## 1.8 Historical Review

Many researchers attempted to design and optimization of combined magnetic deflector and lens systems with minimum aberrations, for examples:

[**Munro** (1974)] derived the formula for calculating the first-order optical properties, third-order aberrations coefficient, and first-order chromatic aberrations for magnetic combined deflective focusing system. His formulae are applicable to the general case in which the lens and deflector field are superimposed on one another.

[**Munro** (1975)] introduced the methods for computing the optical properties of any combination of magnetic lenses and deflection yokes, including the most general case in which the lens and deflector fields may physically be superimposed.

[**Ohiwa** (1977)] presented the considerations and results of designing air-core scanning systems comprising round lenses and saddle type deflection coils.

[**Kuroda** (1980)] introduced the method for calculating the deflective aberration for deflection system with two deflectors and a lens by using the independent aberration of each deflector. The method gives the deflective aberrations without the calculation of deflection fields or paraxial trajectories when the conditions (rotation angle and coil current) of each deflector are changed.

The numerical analysis of magnetic deflector in electron beam lithography system was carried out by [**Munro and Chu** (1981b)]. Formulae were derived for calculating the first and third harmonic components of the magnetic deflection field, for both toroidal and saddle yokes, either in free- space region by using the Biot- Savard law on in

presence of rotationally symmetric ferromagnetic materials by using the finite element method.

A combined system consisting of round lenses and magnetic deflector with superimposed fields had been studied by [**Jiye** (1981)]. The general expressions for superimposed fields and trajectories were obtained. The Gaussian optical properties of the system were discussed and the effect of magnetic deflector on the round magnetic and electrostatic lens might be considered as the linear transformations for Gaussian trajectory parameters. Then the expressions for calculating the aberrations were given in a compact matrix form appropriate for numerical computation.

A focusing and deflection system with vertical landing and reduced aberrations was developed by [**Kuroda et al**(1983)], for direct electron-beam lithography. The system consisted of two magnetic lenses and a magnetic deflector. The excitations of the lenses were opposite to each other. The deflector, which had saddle coils, was set inside the first lens.

[**Lencova** (1988)] summarized some basic ideas used in the design of combined deflection and focusing system.

The fifth order aberration coefficient formulas for deflective focusing systems have been derived by several authors; [**Yu Li et al** (1993)]; [**Uno Y** (1995)]; and [ **Kangyan** and **Tang** (1999)].

[**Wang et al** (2000)] developed differential algebraic method (DA), which implement the DA method to arbitrary high order in visual  $C^{++}$ , and applied it to the analysis of electron lenses and deflection systems separately.

[**Wang** (2002)] introduced a new mathematical method, differential algebraic (DA) method, into the aberration of combined focusing-deflection

system. This method is first introduced by **Berz** (1989) into accelerator physics and achieved great success.

[**Teruo Hosokawa** (2002)] derived the relationships between the third- and fifth-order complex aberration coefficients in electron optical deflective focusing system.

[**Alamir** (2003)] computed the spiral distortion of magnetic lenses with field distribution in the form of an inverse power law.

[**Alamir** (2004)] computed the chromatic aberration of magnetic lenses with a field distribution in the form of an inverse power law.

[**Alamir** (2005)] calculated the optical properties of monopole, multipole magnetic lenses.

[**Yan Ren et al** (2007)] studied the aberration theory of combined electron focusing-deflection system with a rotating deflection field following the rotation of the electron.

## **1.9 Optimization Methods**

The desire to produce electron and ion optical systems with prescribed optical properties and as small aberrations as possible is as old as electron and ion optics itself [**Szilagyi 1988**].

Optimization is the search for such electron and ion optical element that would provide the required optical properties with minimum aberrations. There are two different approaches to optimization: **analysis** and **synthesis**.

The method of analysis is based on trail and error. The designer starts with certain set of given elements (electrodes or pole pieces) and tries to improve their performance by analyzing the optical properties and varying the geometrical dimensions as well as the electric or magnetic parameters of

the system until a satisfactory performance is achieved. Owing to the infinite number of possible configurations this procedure is extremely slow and tedious. It can yield quick and reliable results only if a reasonable guess of the design is already available before the work starts[Szilagyi 1988].

Optimization by synthesis has always been one of the most ambitious goals of electron and ion optics. This approach is based on the fact that any imaging field, its optical properties and aberrations are always totally determined by axial field distribution.

## **1.10 Aim of the Thesis**

The aim of this work is to find the optimum design of magnetic system which consists of magnetic deflector and lens which gives rise to the minimum spherical, chromatic, spiral distortion and radial distortion aberration. The synthesis approach of optimization method is used in the present work.

In the calculations; the toroidal deflection coil is used as the source of magnetic field, then the exponential field distribution model is used. Also, the moving objective lens concept is included in the computation of deflection field.

Deflection aberrations can be minimized for the exponential field distribution model by changing the shape of the deflection coil, where the length and angle can be varied. By using the optimum axial field distribution, the pole pieces design which gives rise to this field distribution can be found by using reconstruction method.

Chapter

*Two*



*Theoretical  
2  
Considerations*

# Chapter Two

## Theoretical Considerations

### 2.1 Introduction

A charge particle beam is a group of particles that have about the same kinetic energy and move in about the same direction [Humphries 2002]. The high kinetic energy and directionality of charged particles in beams make them useful for applications.

Charged particle beams have continually expanding applications in many branches of research and technology. Recent active areas include flat-screen cathode-ray tubes, and beam lithography for microcircuits.

### 2.2 Paraxial-Ray Equation in Magnetic Fields

The paraxial ray equation in axially symmetric magnetic fields can be written as [Tsimring 2007]:

$$\frac{d^2r}{dz^2} + \frac{eB_0^2(z)}{8mV_r} r = 0 \quad (2-1)$$

where  $e$  and  $m$  are the charge and mass of electron respectively, and  $V_r$  is the relativistically corrected accelerating voltage which is given by [Szilagy 1988].:

$$V_r = (1 + 0.978 \times 10^{-6} V_a) \quad (2-2)$$

where  $V_a$  is the accelerating voltage.

Equation (2-1) is a second order differential equation. This equation was solved numerically using Range-Kutta-Nystrom method [Kreyszig 1983]. In present work we check our results to solve the equation (2-1) analytically by the method of undetermined coefficients using MATLAB program [Karris 2004].

### 2.3 Optical Parameters and Initial Conditions

Some definitions of the optical parameters used in the present work are given in this section.

Object side: The side of optical design at which the charged particles enter.

Image side: The side of optical design at which the charged particles leave.

The object plane ( $Z_o$ ): The plane at which the physical object is placed, or a real image is formed from a previous optical design, on the object side.

The image plane ( $Z_i$ ): The plane at which the real image of the object plane  $Z_o$  is formed, on the image side.

Focal length (F): The focal length is the distance between the principle plane and the focus [Tsimring 2007].

Magnification (  $M$  ): In any optical system the ratio between the transverse dimension of the final image and the corresponding dimension of the original object is called the lateral magnification " $M$ ":



$$M = \frac{\text{image height}}{\text{object height}} \quad (2-3)$$

There are three magnification conditions under which an optical design such as lens or deflector can operate, namely [Munro 1975]:

- (i) zero magnification condition: In this operational condition  $Z_o = -\infty$  as shown in figure (2-1). As an example, the final probe-forming lens in a scanning electron microscope (SEM) is usually operated under this condition.



**Figure (2-1): Zero magnification condition.**

- (ii) Infinite magnification condition: In this case  $Z_i = +\infty$  as shown in figure (2-2). As an example, the objective lens in a transmission electron microscope (TEM) is usually operated under this condition.

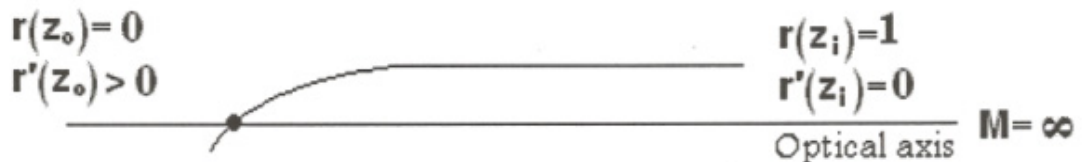


**Figure (2-2): Infinite magnification condition.**

(iii) Finite magnification condition: Under this operational condition  $Z_o$  and  $Z_i$  are at finite distances, as shown in figure (2-3). As an example the electrostatic lens in field-emission gun is usually operated under this condition.

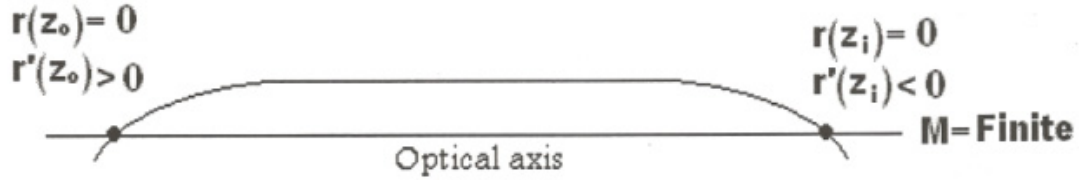


*Figure (2-3): Finite magnification condition.*

## 2.4 Magnetic Deflection Fields

In magnetic deflector, two geometries are common: saddle and toroidal coils. In the present work, the toroidal coil is taken as the source of magnetic field.

The method used for calculating the deflection yoke fields depends on whether the deflection coils are near the magnetic materials or not [Septier 1980]. If the deflection yoke is in a free-space region, its field can be calculated using the Biot-savart's formula. The deflection field at the axis of an air-cored toroidal coil,  $\mathbf{B}_x(\mathbf{z})$ , is obtained using the formula given by [Munro 1975]:

$$B_x(z) = \frac{NI\mu_0 \sin \varnothing}{\pi} \left[ \frac{\sqrt{l^2 + r^2}}{lr} - \frac{\sqrt{h^2 + r^2}}{hr} + \frac{\sqrt{h^2 + R^2}}{hR} - \frac{\sqrt{l^2 + R^2}}{lR} \right] \quad (2-4)$$

where  $NI$  is the magnetic excitation,  $\emptyset$  is the angle of the toroidal coil,  $R$  and  $r$  are the outer and inner radius of the toroidal coil, respectively,  $B_x(z)$  is deflection field of toroidal yoke and  $h$  and  $l$  are defined in figure (1-1).

If the deflection coil is near magnetic materials, the Biot-savart's formula is no longer applicable. Instead, some numerical technique must be used, such as the finite-element method. This method can be used for either toroidal or saddle yokes, wound on magnetic formers or placed inside magnetic circuits.

## 2.5 Magnetic Scalar Potential Calculation

The magnetic scalar potential is an essential factor for finding the pole piece shape. Thus, it is important to determine the magnetic scalar potential distribution along the lens and deflector system length. At the lens axis the axial flux density distribution is given by. [Al-Obaidi1995].

$$B_z = -\mu_0 \frac{dV_z}{dz} \quad (2-5)$$

where  $B_z$  is the axial flux density distribution,  $V_z$  is the axial potential distribution, and  $\mu_0$  is the permeability of free space. The magnetic scalar potential  $V_z$  can be calculated by integrating equation (2-5) along the lens and deflector system axis.

$$\int_a^b dV_z = -\frac{1}{\mu_0} \int_a^b B_z dz \quad (2-6)$$

i.e.,

$$V_{zb} - V_{za} = -\frac{1}{\mu_0} \int_a^b B_z dz \quad (2-7)$$

where a and b are the axial magnetic field limits.

It is intended to find the magnetic scalar potential along the lens and deflector system as a tabulated data set. Thus the lens and deflector system axis (i.e. the interval where the axial magnetic field exists) is divided into (n-1) subintervals where n is the number of points (z , B<sub>z</sub>). The axial magnetic flux density B<sub>z</sub> can be approximated by the well-known cubic spline for each subinterval as follows:

$$B_z = B_i + B'_i(z - z_i) + 0.5B''_i(z - z_i)^2 \frac{B''_{i+1} - B''_i}{6(z_{i+1} - z_i)} (z - z_i)^3 \quad (2-8)$$

where  $z_i \leq z \leq z_{i+1}$ , and  $i = 1, 2, 3, \dots, (n-1)$ . Equation (2-6) can be executed over each subinterval with the aid of equation (2-8); the result is the following recurrence formula,

$$V_{z(i+1)} = V_{zi} - \mu_0^{-1} \left[ B_i h_i + B'_i \left( \frac{h_i^2}{2} \right) + B''_i \left( \frac{h_i}{2} \right)^3 + \left( \frac{B''_{i+1}}{3} \right) \left( \frac{h_i}{2} \right)^3 \right] \quad (2-9)$$

where  $h_i = (z_{i+1} - z_i)$  is the width of each subinterval. Equation (2-9) can be written in the following simplified form

$$V_{z(i+1)} = V_{zi} - E_i \quad (2-10)$$

Where

$$E_i = \mu_0^{-1} \left[ B_i h_i + B_i' \left( \frac{h_i^2}{2} \right) + B_i'' \left( \frac{h_i}{2} \right)^3 + \left( \frac{B''_{i+1}}{3} \right) \left( \frac{h_i}{2} \right)^3 \right]$$

Since the axial magnetic flux density considered in this work is symmetrical, one can put

$$V_{z(n-1)} = -V_{zi} = 0.5NI$$

The recurrence formula (2-10) can thus be written in the following form,

$$V_{z(i+1)} = -0.5NI - E_i \quad (2-11)$$

for each subinterval  $z_i \leq z \leq z_{i+1}$ . Therefore, one can get the magnetic scalar potential  $V(z)$  along the lens and deflector system interval  $z_i \leq z \leq z_n$ . The above algorithm has been formulated into a MATLAB 2008.

## 2.6 Pole Piece Reconsideration

The pole piece shape can be design by using the following equation,

$$R_p(z) = 2 \left[ \frac{(V_z - V_p)}{V_z''} \right]^{1/2} \quad (2-12)$$

where  $R_p$  is the radial height of the pole piece and  $V_p$  is the value of the potential of the pole piece.

This equation used by [Szilagyi 1984] to reconstruct the pole piece shape of magnetic deflector and lens.

## 2.7 The Moving Objective Lens (MOL) Concept

The concept of moving objective lens (MOL) was introduced first by [Ohiwa et al 1971]. Ohiwa pointed out that the aberrations of a combined focusing and deflection system can be greatly reduced by using an arrangement of the type shown in figure (2-4).

A point source of electrons, emitted from  $z_0$ , is imaged by a lens at  $z_i$ . The beam is deflected by the first deflector so that it enters the lens off axis, a second deflector, placed inside the lens. This so-called "moving objective lens" (MOL) reduces the effect of the off axis lens aberrations. The spherical and chromatic aberration of the lens can be kept small by having a short working distance  $L_2$  (see figure 2-4). At the same time the deflection aberrations can be kept small by having a large distance  $L_1$  from the first deflector to the image plane [Marton 1980]. This concept has been analyzed theoretically by [Ohiwa et al. 1971] and [Goto and Soma 1977], and has been used in practical designs by [Munro 1975], [Ohiwa 1978], and [Goto et al. 1978].

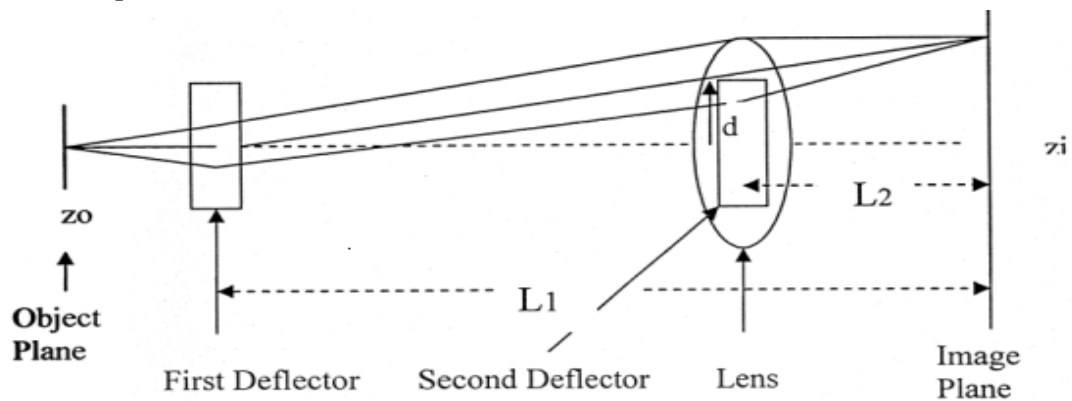


*Figure (2-4) The moving objective lens concepts [Ohiwa 1978].*

Let  $B(z)$  the axial flux density distribution for lens and  $D(z)$  the deflection flux density required at the axis. Then, the following relation holds [ **Ohiwa 1978 and Lencova 1987**].

$$D(z) = \frac{1}{2} dB'(z) \quad (2- 13)$$

where  $d$  is the displacement by the first deflector (pre deflection).

## **2.8 Aberrations of Axially Symmetric Electron Optical Systems**

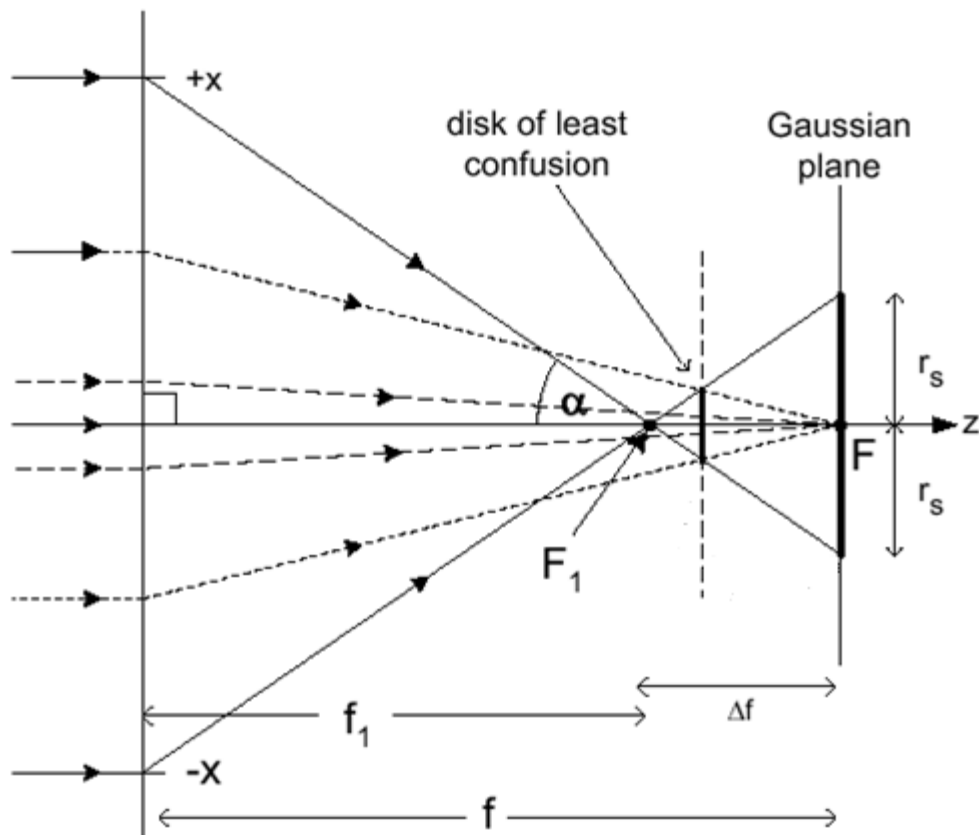
The theory of aberrations is the most extensively studied area in both light optics and electron optics. Intensive investigations of aberrations in axially symmetric electron-optical systems were carried out since the 1930 in connection with studies of the electron transmission microscope problem. Their implementation provides the creation of an ideal lens that forms stigmatic and similar images. Let us recall these assumptions: (1) rigorous axial symmetry; (2) paraxial trajectory approximation; (3) energy homogeneity, including the absence of time-dependent processes; and (4) negligible space-charge fields and small effects of electron diffraction. Violation of at least one of these conditions leads to aberrations that are responsible for blurred or distorted images and complicate beam transport problems [ **Tsimring 2007**].

### **2.8.1 Spherical Aberration**

The spherical aberration is one of the most important geometrical aberrations; result from violation of paraxial trajectory approximation.

The problem of spherical aberration is fundamental in electron microscopy, in which objects are very small and arranged close to the optical axis [ **Tsimring 2007**].

The effect of spherical aberration can be defined by means of the a diagram that shows electrons arriving at a lens after traveling parallel to the optic axis but not necessarily along it; see figure (2-5). Those that arrive very close to the optic axis (paraxial rays, represent by dashed lines in figure (2-5)) are brought to a focus  $F$ , a distance  $f$  from the center of the lens, at the Gaussian image plane. When spherical aberration is present, electrons arriving at an appreciable distance  $x$  from the axis are focused to a different point  $F_1$  located at a shorter distance  $f_1$  from the center of the lens[Egerton 2007].



***Figure(2-5):Definition of the disk of confusion due to spherical aberration, in terms of focusing parallel rays by a lens [Egerton 2007].***



When these non-paraxial electrons arrive at the Gaussian image plane, they will be displaced radically from the optic axis by an amount  $r_s$  given by [Egerton 2007].:

$$r_s = C_s \alpha^3 \quad (2-14)$$

where  $C_s$  is the spherical aberration coefficient .

Figure (2-5) illustrates a limited number of off-axis electron trajectories, the formation of an aberration circle, with electrons arriving at the lens with all radial displacements (between zero and some value  $x$ ) within the  $x$ - $z$  plane, within the  $y$ - $x$  plane (perpendicular to the diagram), and within all intermediate planes that contain the optic axis. Due to the axial symmetry, all these electrons arrive at the Gaussian image plane within the disk of confusion (radius  $r_s$ ) [Egerton 2007].

The spherical aberration coefficient  $C_s$  of an axially symmetric magnetic optical element is given by [Tahir 1985]:

$$C_s = (e/128mV_r) \int_{z_0}^{z_i} r^4 \left\{ (3e/mV_r) B^2(z) + 8B'^2(z) - 8B^2(z)(r'/r)^2 \right\} dz \quad (2-15)$$

where  $r$  is the solution of the paraxial-ray equation with an initial condition depending on the operation mode. The integration covers the whole interval from object plane  $z_0$  to image plane  $z_i$ .

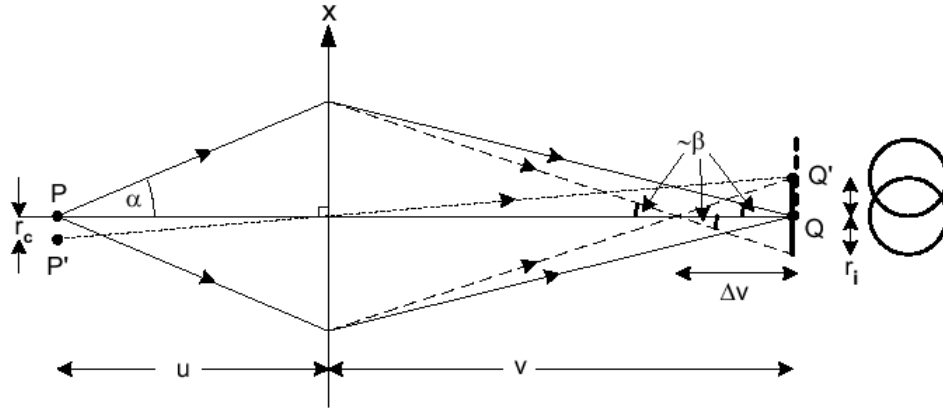
## 2.8.2 Chromatic aberration

In light optics, chromatic aberration occurs when there is spread in the wavelength of the light passing through a lens, coupled with a variation of the refractive index with wavelength (dispersion). In the case of an electron, the de Broglie wavelength depends on the particle momentum, and therefore on its kinetic energy  $E_0$ . So if electrons are present with different kinetic energies, they will be a chromatic disk of confusion rather than a point focus. The spread in kinetic energy can arise from several causes.

- 1-Different kinetic energies of the electrons emitted from the source. For example, electrons emitted by a heated-filament source have a thermal spread ( $\approx k T$ , where  $T$  is the temperature of the emitting surface) due to the statistics of the electron-emission process.
- 2-Fluctuation in the potential  $V_0$  applied to accelerated electrons. Although high-voltage supplies are stabilized as well as possible, there is still some drift (slow variation) and ripple (alternating component) in the accelerating voltage, and therefore in the kinetic energy  $e V_0$ .
- 3-Energy loss due to inelastic scattering in the specimen, a process in which energy is transferred from an electron to the specimen. This scattering is also a statistical process: not all electrons lose the same amount of energy, resulting in an energy spread within the transmitted beam.

Consider an axial point source  $P$  of electrons (distance  $u$  from the lens) that is focused to a point  $Q$  in the image plane (distance

v from the lens) for electrons of energy  $E_0$  as shown in figure (2-6).



**Figure(2-6):Ray diagram illustrating the change in focus and the disk confusion resulting from chromatic aberration. With tow object points, the image disks overlap [Egerton 2007] .**

Electron of energy  $E_0 - \Delta E_0$  will have in image distance  $v - \Delta v$  and arrive at the image plane a radial distance  $r_i$  from the optic axis. If the angle  $\beta$  of the arriving electrons is small[Egerton 2007].

$$r_i = \Delta v \tan \beta \approx \beta \Delta v \quad (2-16)$$

The loss of spatial resolution due to chromatic aberration is therefore [Egerton 2007].

$$r_c \approx \alpha C_c (\Delta E_0 / E_0) \quad (2-17)$$

where  $C_c$  is the chromatic aberration coefficient [Egerton 2007].

The chromatic aberration coefficient  $C_c$  of an axially symmetric magnetic optical element is given by [Tahir 1985]:

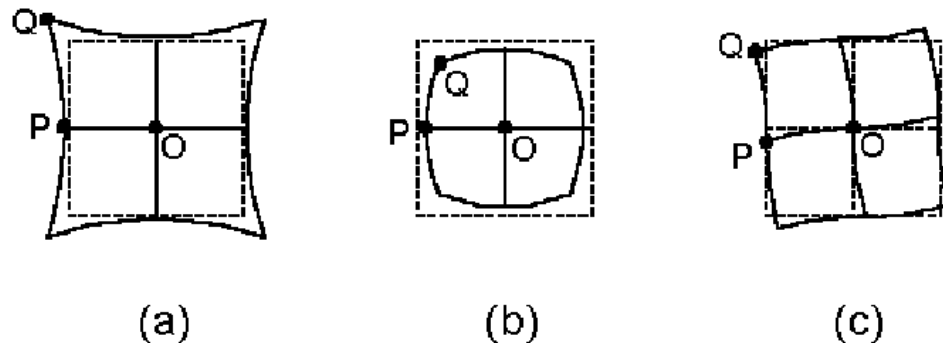
$$C_c = (e/8mV_r) \int_{z_0}^{z_i} B^2(z) h^2(z) dz \quad (2-18)$$

The integration covers the whole interval from object plane  $z_o$  to image plane  $z_i$ .

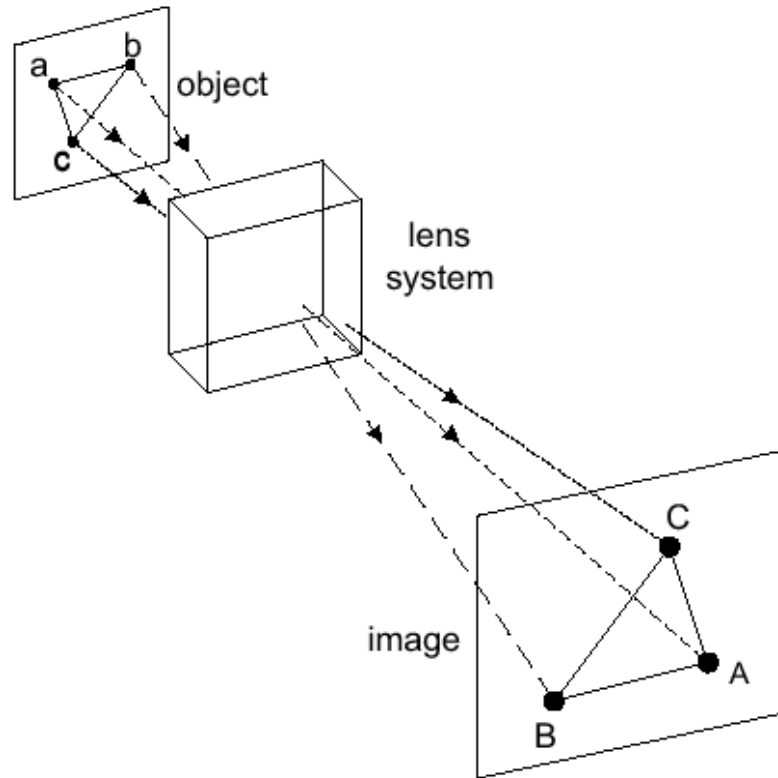
### 2.8.3 Radial and spiral distortions

The presence of image distortion is equivalent to a variation of the magnification factor with position in the object or image there are: two types of radial distortion Pincushion distortion and barrel distortion.

The pincushion distortion corresponding to  $M$  increasing with radial distance away from optical axis as in figure (2-6a), barrel distortion corresponds to  $M$  decreasing away from the axis as in figure (2-7b). Many electron lenses cause a rotation of the image, and if this rotation increases with distance from the axis, the result is spiral distortion figure (2-7c) and (2-8) [Egerton 2007].



**Figure(2-7):(a) Square mesh (dashed lines ) image with pincushion distortion (solid curves); magnification  $M$  is higher at point  $Q$  than that at point  $p$ . (b) Image showing barrel distortion, with  $M$  at  $Q$  lower than at  $P$ . (c) Image of a square, showing spiral distortion; the counterclockwise rotation is higher at  $Q$  than at  $P$  [Egerton 2007].**



***Figure(2-8): A triangle imaged by an ideal lens, with magnification and inversion. Image point A, B, and C are equivalent to the object points a, b, and c, respectively***

**[Egerton 2007].**

In an undistorted image, the distance  $R$  of an image point from the optic axis is given by  $R = M r$ , where  $r$  is the distance of the corresponding object point from the axis, and the image magnification  $M$  is a constant. Distortion changes this ideal relation to[Egerton 2007]:

$$R = Mr + Dr^3 \quad (2-19)$$

where  $D$  is distortion coefficient ( $D_{sp}$  for spiral distortion and  $D_{rad}$  for radial distortion).

If  $D > 0$ , each image point is displaced outwards, particularly those further from the optical axis, and the entire image suffers from pincushion distortion figure as in (2-7a). If  $D < 0$ , each image point is displaced inward relative to the ideal image and barrel distortion is present as in figure (2-7b).

For most purposes, distortion is a less serious lens defect than aberration (spherical and chromatic aberrations), because it does not result in a loss of image detail. In fact, it may not be noticeable unless the microscope specimen contains straight-line feature [Egerton 2007].

The spiral and radial distortion coefficient of an axially symmetric magnetic optical element is given by [Tsuno 1981]:

$$D_{sp} = \left(\frac{1}{16V_r}\right) \cdot \left(\frac{2e}{mV_r}\right)^{1/2} \int_{-\infty}^{\infty} B(z) \left\{ \left(\frac{3e}{8m}\right) B^2(z) + V_r \left(\frac{Y'}{Y}\right) \right\} Y^2 dz \quad (2-20)$$

$$D_{rad} = \frac{3}{8f_p^2} \left(\frac{2e}{16mV_r}\right) \int_{-\infty}^{\infty} \left\{ B'^2(z) + \left(\frac{3e}{8mV_r}\right) \times B^4(z) - B^2(z) \left(\frac{Y'}{Y}\right)^2 \right\} Y^3 X dz \quad (2-21)$$

where, x and y are two independent solutions of the paraxial-ray equation with an initial condition depending on the operation

mode, the primes denote derivatives with respect to  $z$  and  $f_p$  is the projector focal length .

Chapter

**Three**



3  
Results & Discussion



# *Chapter Three*

## Results and Discussion

### **3.1 The Behavior of the Magnetic Deflector and Lens at Different Values of Length and Angle of Coil**

In the present work, the properties of a magnetic system (deflector and lens) have been studied. The toroidal yoke coil is used as the source of the magnetic field. The optimum design is found by changing the geometrical shape of the coil via changing the values of length and angle of the coil to give minimum values of relative spherical, chromatic, spiral distortion and radial distortion aberration coefficients. The exponential function is given by [Hawks1982] used for the shape of magnetic field distribution. The procedure of the calculations is divided into four steps: The first; calculating the magnetic field of the system, second: calculating the trajectory of the electron beam, third calculating the relative spherical, chromatic, spiral distortion and radial distortion aberration coefficients, and forth design the pole piece shape .

### 3.2 Design Using Exponential Model

According to exponential function the axial flux density distribution is given by [Hawks1983]:

$$\mathbf{B}(z) = \mathbf{B}_m \exp - (z/a)^2 \quad (3-1)$$

where  $B_m$  is the maximum value of magnetic field,  $z$  is the length of the optical axis along the system and it is calculated using eq. (2-4), and  $a$  is the field width at half maximum  $B_m/2$ . The axial flux density distribution of the deflector  $D(z)$  is computed using equation (2-13) where  $B'(z)$  is computed with aid of equation (3-1). The field of deflector, lens and the superimposed field (system field) has been calculated for different values of lengths and angles of the coil as shown in figures (3-1— 3-6). From these figures one can note that when the length and angle of the coil increases the field increases. The field is directly proportional to the length and angle of the coil.

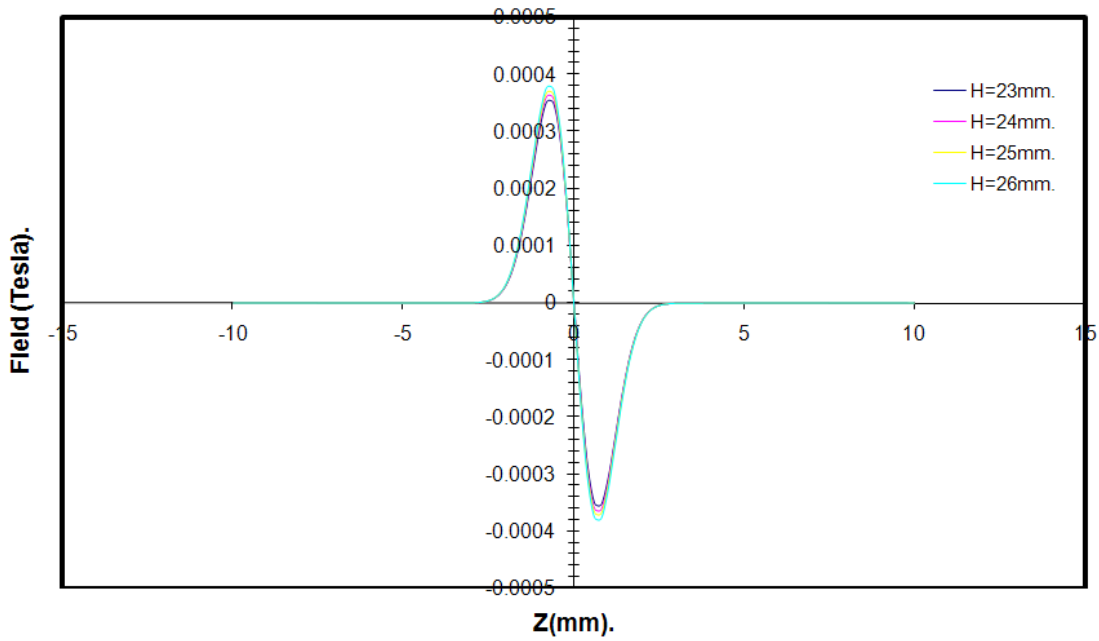


**Figure (3-1):** The field of the magnetic deflector at angle of the coil  $\theta=61^\circ$  for different values of length of the coil.

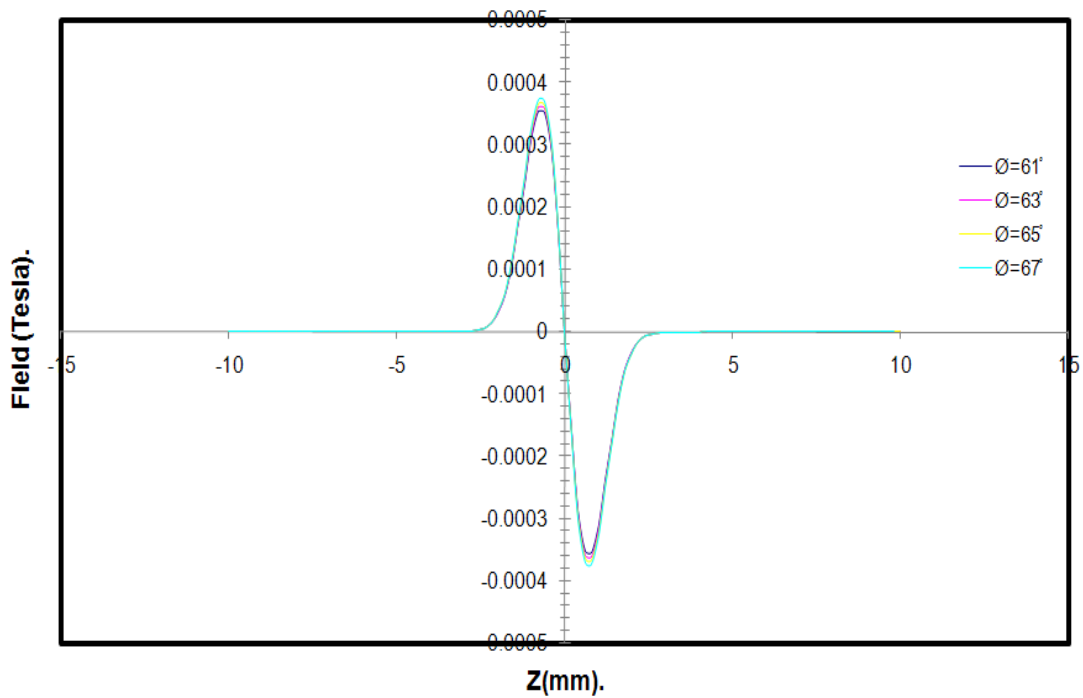


**Figure (3-2):** The field of the magnetic deflector at length of the coil  $H=23$  mm for different values of angle of the coil.

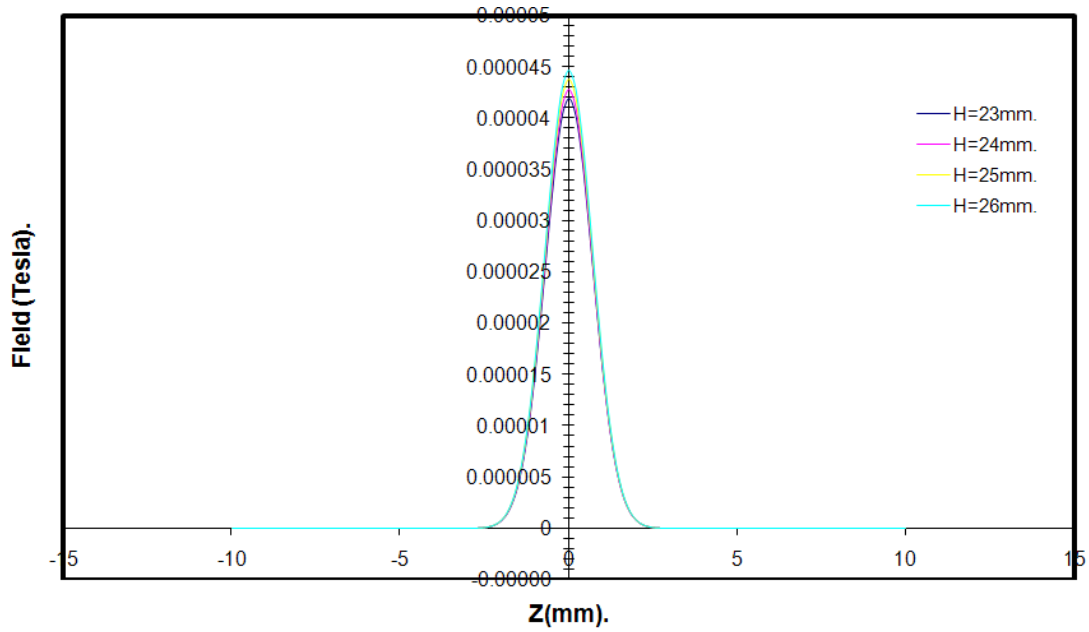


**Figure (3-3):** The field of the magnetic lens at angle of the coil  $\theta=61^\circ$  for different values of length of the coil.

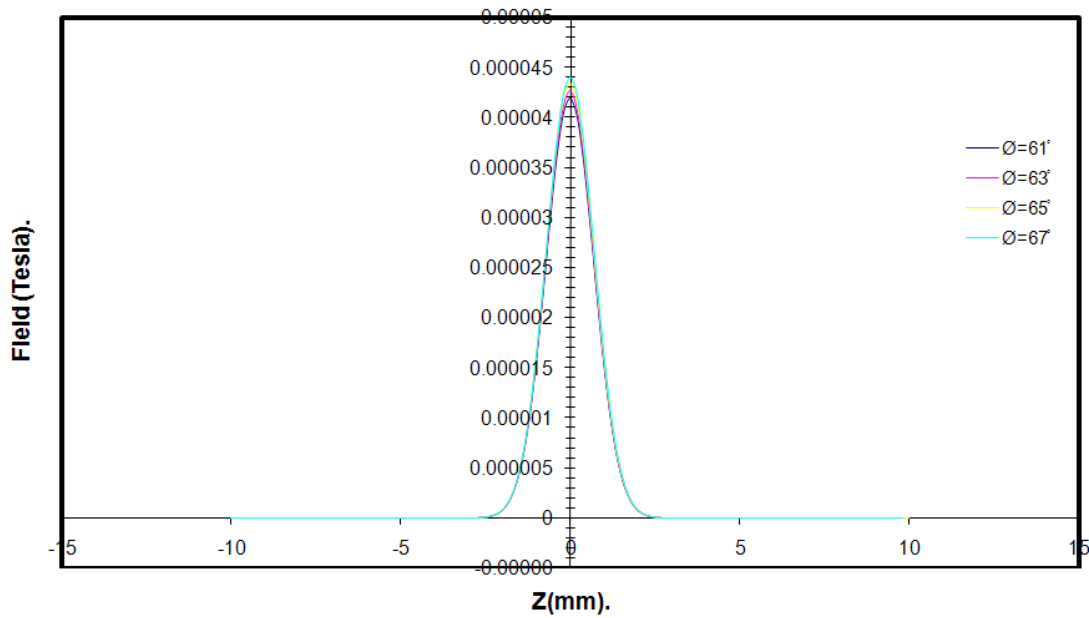


**Figure (3-4):** The field of the magnetic lens at length of the coil  $H=23$  mm for different values of angle of the coil.

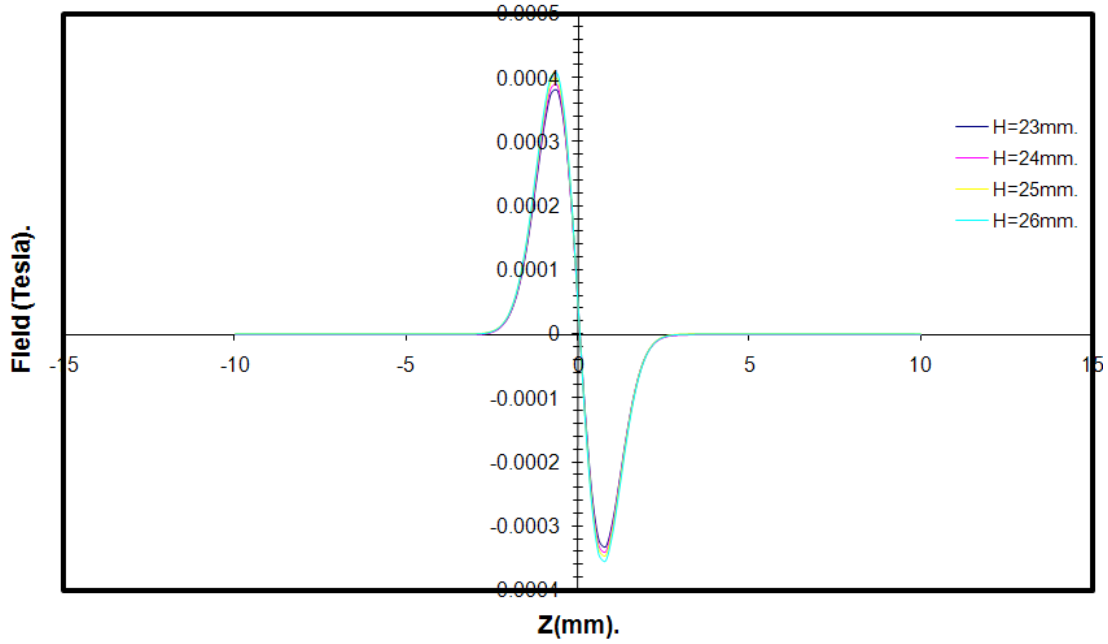


**Figure (3-5):** *The field of the magnetic system at angle of the coil  $\theta=61^\circ$  for different values of length of the coil.*

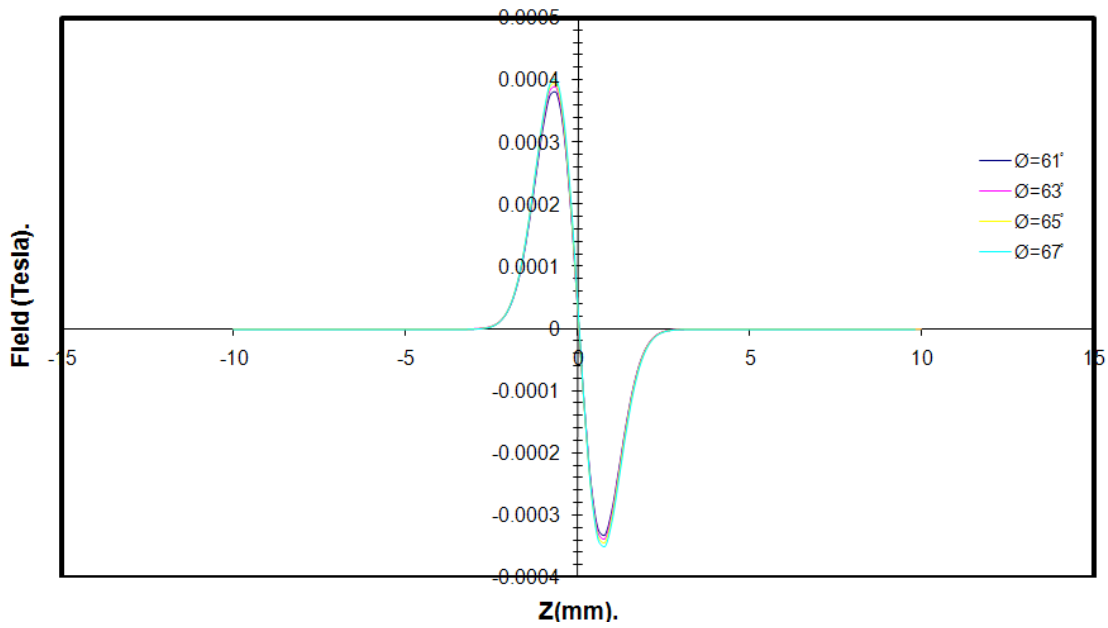


**Figure (3-6):** *The field of the magnetic system at length of the coil  $H=23$  mm for different values of angle of the coil.*

### 3.3 Electron Beam Trajectory

The electron beam path along the magnetic system field under infinite magnification condition has been computed using equation (2-1). Figures (3-7) and (3-8) shows the trajectories of an electron beam traversing the magnetic system field at various values of both length and angle of the coil.

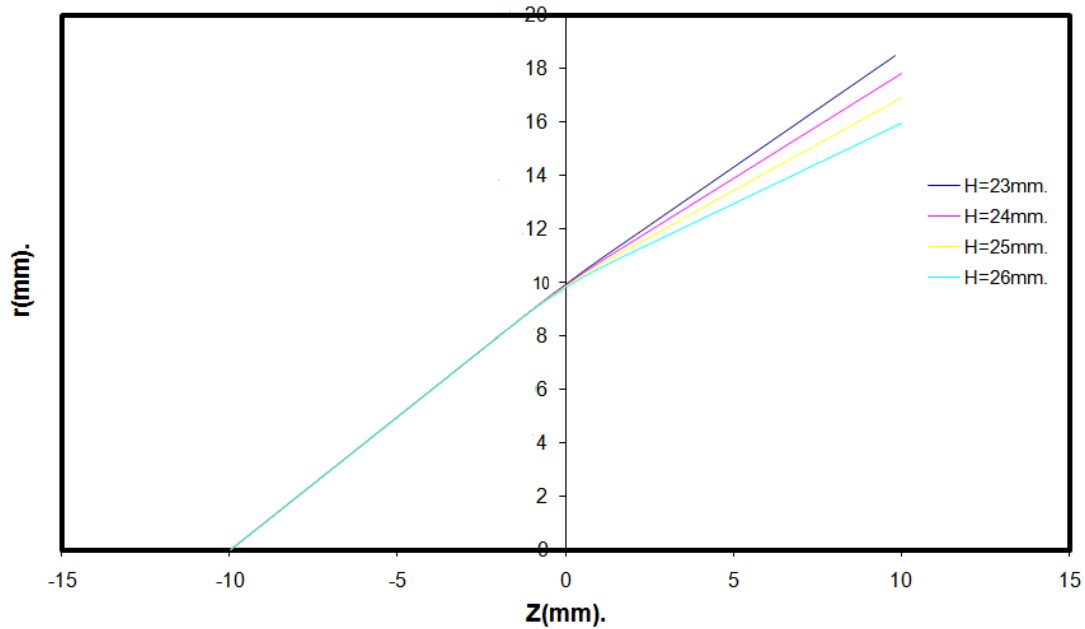


**Figure (3-7):** The electron beam trajectory in the magnetic system under infinite magnification condition at  $NI/(Vr)^{0.5}=32.27$  for the angle of the coil  $\theta=61^\circ$  and different values of length of the coil  $H$ .

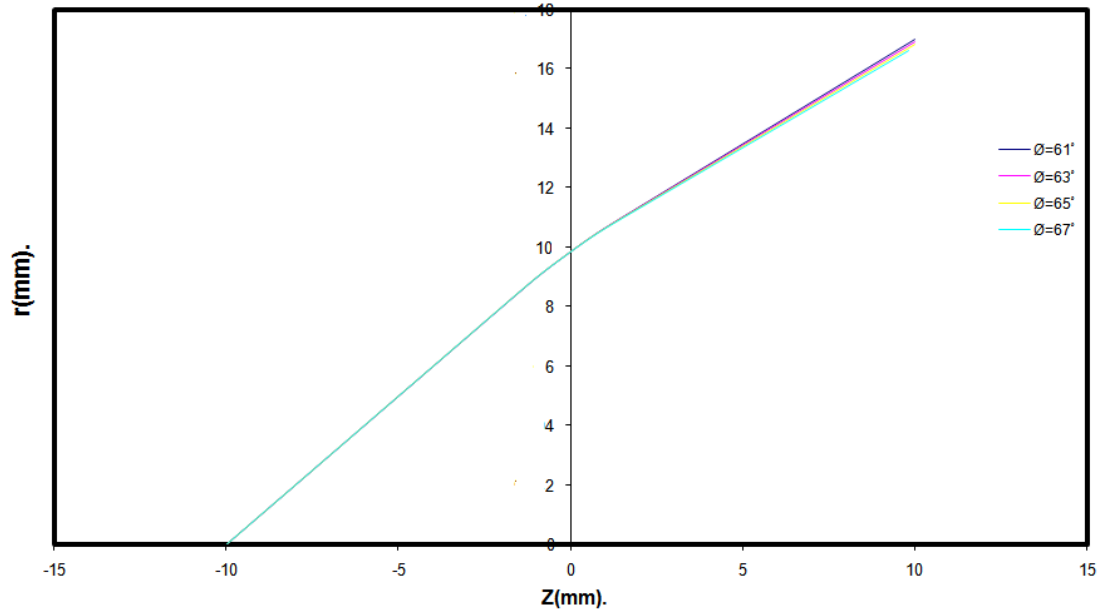


**Figure (3-8):** The electron beam trajectory in the magnetic system under infinite magnification condition at  $NI/(Vr)^{0.5}=32.27$  for the length of the coil  $H=23\text{mm}$  and different values of angle of the coil  $\theta$ .

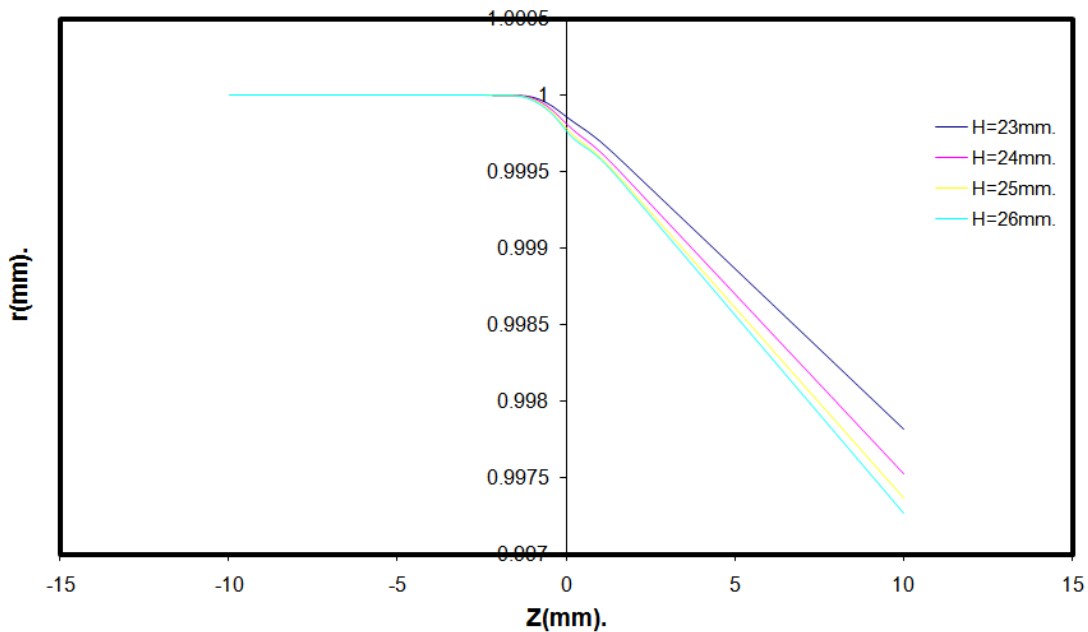


**Figure (3-9):** The electron beam trajectory in the magnetic system under zero magnification condition at  $NI/(Vr)^{0.5}=32.27$  for the angle of the coil  $\theta=61^\circ$  and different values of length of the coil  $H$ .

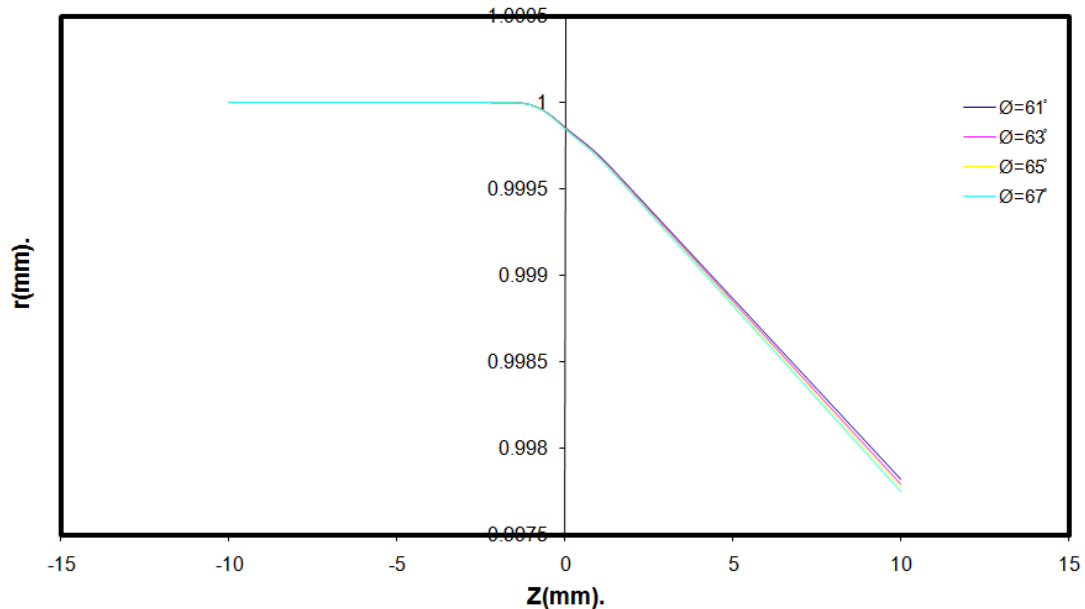


**Figure (3-10): The electron beam trajectory in the magnetic system under zero magnification condition at  $NI/(Vr)^{0.5}=32.27$  for length of the coil  $H=23$  mm and different values of angle of the coil  $\theta$  .**

The effect of the length and angle of coil has been investigated at value of excitation parameter  $NI/(Vr)^{0.5}(=32.27 \text{ Amp.turns}/(\text{volt})^{0.5})$ . Computation has shown that as the beam emerges from magnetic field it diverges away from the optical axis. The trajectories of electron beams are deflecting more away from the optical axis as the values of length of the coil (H) and angle of the coil ( $\theta$ ) decreases. The effect of change the length of the coil (H) and angle of the coil ( $\theta$ ) on the electron beam trajectory is due to the effect of the field of the magnetic system, where as length of the coil (H) and angle of the coil ( $\theta$ ) decrease the field decreasing too as shown in figures (3-5) and (3-6).

Figure (3-9) and (3-10) shows the trajectory of an electron beam traversing the magnetic field of the system at various values of the length of the coil (H) and angle of the coil ( $\theta$ ). These trajectories have been



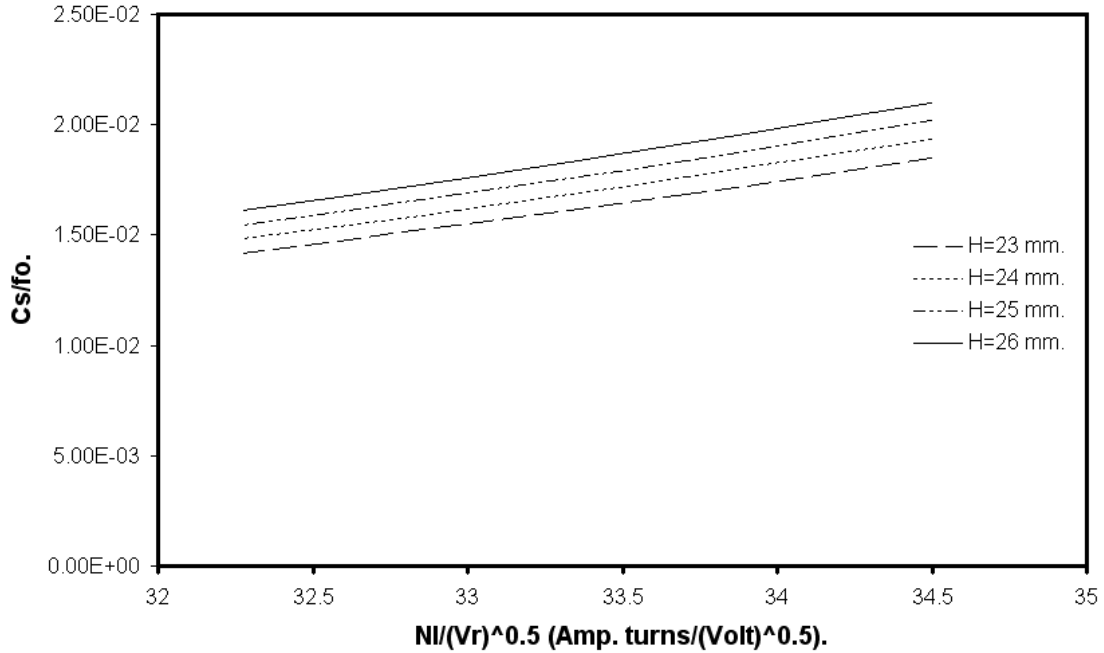
computed with the aid of equation (2-1) under zero magnification condition and the constant value of the excitation parameter  $NI/(Vr)^{0.5} = 32.27$  Amp. turns/(volt)<sup>0.5</sup>. The computation shows that the beam emerges from system field converges near the optical axis. The trajectories of electron beams are deflect near the optical axis as the values of length of the coil (H) and angle of the coil ( $\emptyset$ ) increases. The effect of changing the length of the coil (H) and the angle of the coil ( $\emptyset$ ) on the electron beam trajectory is due to the effect of the magnetic field , where as length of the coil (H) and angle of the coil( $\emptyset$ ) increases the field is increasing too as shown in figures (3-5) and (3-6).

### **3.4 Infinite Magnification Condition**

#### **3.4.1 Effects of changing the length**

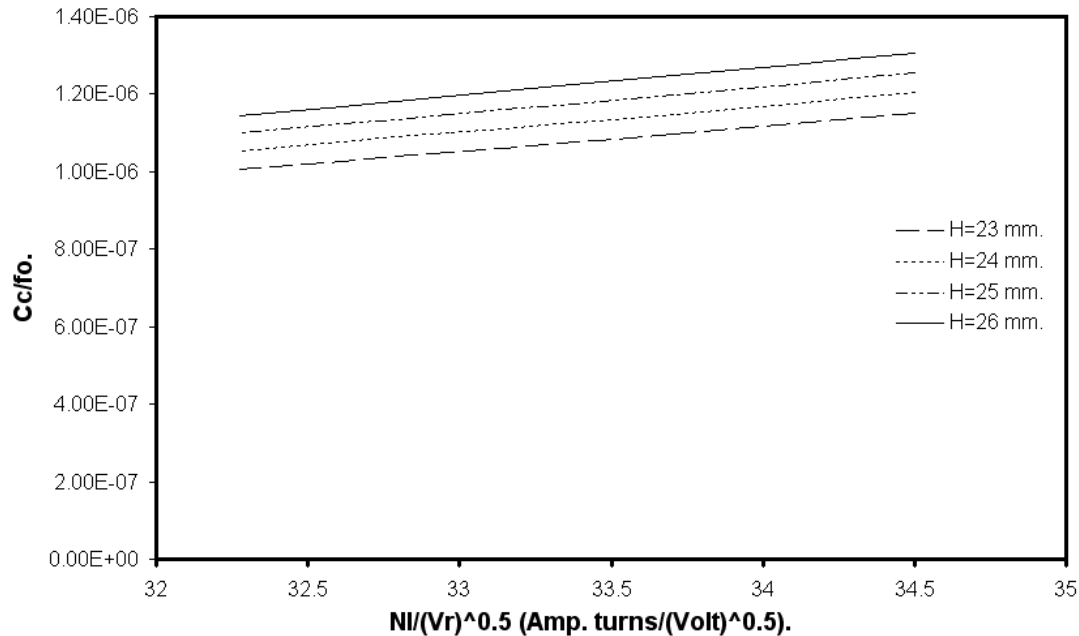
##### **a- Relative spherical and chromatic aberration coefficients**

To study the effects of variation of the length of the coil (H) on the spherical and chromatic aberration coefficients  $C_s/f_o$  and  $C_c/f_o$ . the different values of the length of the coil H=23, 24, 25 and 26mm with angle of the coil  $\emptyset = 61^\circ$  are taken into account. Figure (3-11) shows this effect on the spherical aberration coefficient. This figure shows that the length H=23mm gives the lower value of spherical aberration coefficient  $C_s/f_o$  .



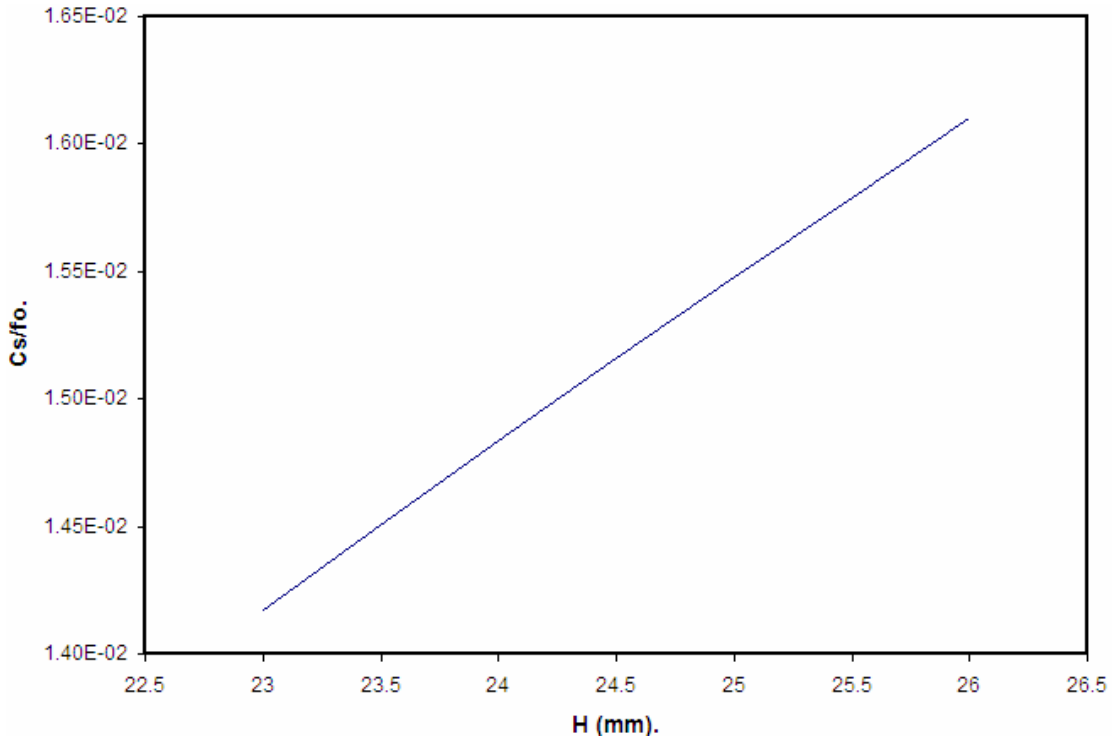
**Figure (3-11): The relative spherical aberration coefficient  $C_s/f_o$  as a function of  $NI/(Vr)^{0.5}$  for the angle of the coil  $\theta=61^\circ$  and the lengths of the coil  $H= 23, 24, 25$  and  $26$  mm.**

Figure (3-12) shows the effect of variation of the length of the coil (H) on the chromatic aberration coefficient  $C_c/f_o$ . Figure (3-12) shows that the length of the coil  $H=23$ mm gives the best value of chromatic aberration coefficient  $C_c/f_o$ . In both spherical and chromatic aberration coefficients one can find that the values of relative aberration coefficient increase as the ratio of the excitation parameter  $NI/(Vr)^{0.5}$  increases. Also, at the lower values of the excitation parameter  $NI/(Vr)^{0.5}$  one has the best values of both spherical and chromatic aberration coefficients, and one can select the values of NI and Vr to keep this ratio small.



**Figure (3-12): The relative chromatic aberration coefficient  $C_c/f_o$  as a function of  $NI/(Vr)^{0.5}$  for the angle of the coil  $\theta=61^\circ$  and the lengths of the coil  $H= 23, 24, 25$  and  $26$  mm.**

The relation between spherical and chromatic aberration coefficients  $C_s/f_o$  and  $C_c/f_o$  and the length of the coil (H) is shown for the excitation parameter  $NI/(Vr)^{0.5}=32.27$  Amp. turns/(volt)<sup>0.5</sup> in figures (3-13) and (3-14), respectively. The values of spherical and chromatic aberration coefficients  $C_s/f_o$  and  $C_c/f_o$  increase when the length of the coil (H) increases and at the length  $H=23$ mm one can find the best result. Therefore, to reduce the values of relative spherical and chromatic aberration coefficients the designer can use the shorter lengths to design the toroidal deflection coil.



**Figure (3-13):** The relative spherical aberration coefficient  $C_s/f_o$  as a function of the coil length ( $H$ ) for the angle of the coil  $\theta=61^\circ$ .

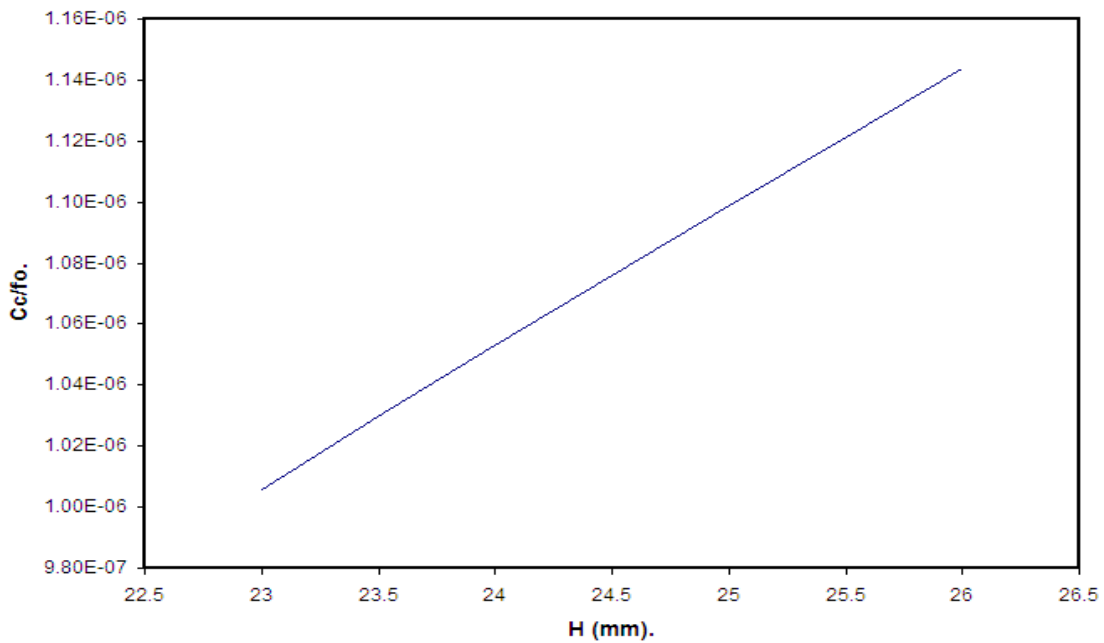


**Figure (3-14):** The relative chromatic aberration coefficient  $C_c/f_o$  as a function of the coil length ( $H$ ) for the angle of the coil  $\theta=61^\circ$ .

## b- Relative radial and spiral distortion coefficients

Figure (3-15) shows the relative radial distortion coefficient  $D_{rad} * f_p^2$  of the magnetic system as a function of the excitation parameter  $NI/(Vr)^{0.5}$ .

From the figure (3-15) one can note the values of the relative radial distortion coefficients  $D_{rad} * f_p^2$  are decreasing as the length of coil (H) decreases. Also the values of the relative radial distortion coefficients  $D_{rad} * f_p^2$  increase as the excitation parameter  $NI/(Vr)^{0.5}$  increases. The best values of the radial distortion coefficients  $D_{rad} * f_p^2$  occur at the low values of the excitation parameter  $NI/(Vr)^{0.5}$  and the length of the coil  $H = 23$  mm and  $\theta = 61^\circ$  gives the minimum values of the aberration coefficients.

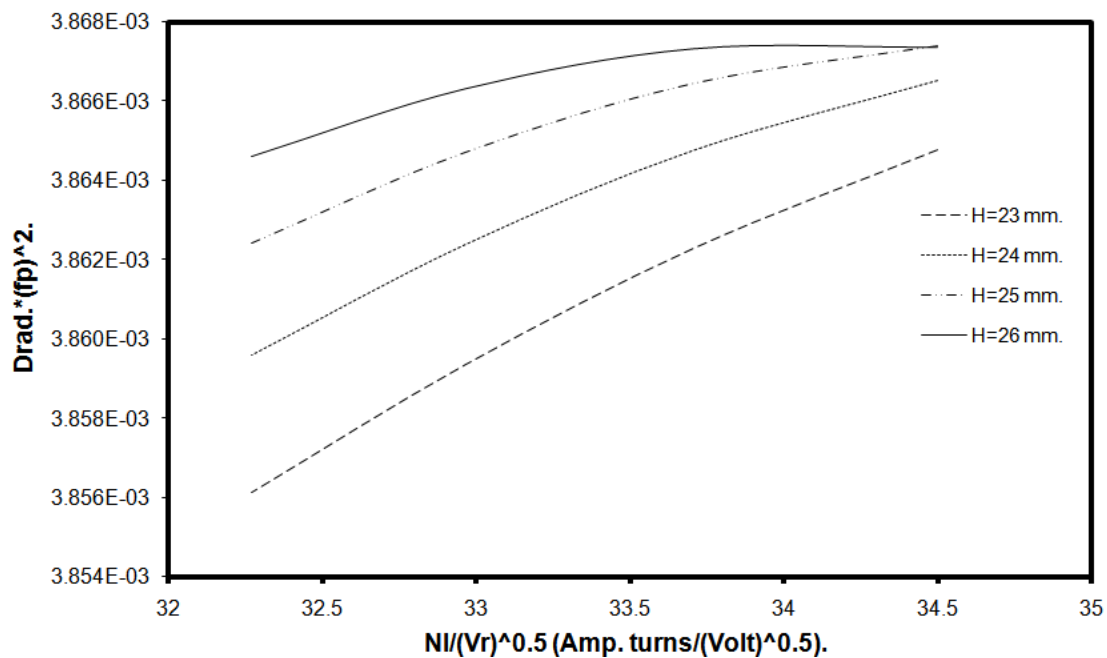


**Figure (3-15):** The relative radial distortion coefficient  $D_{rad} * f_p^2$  as a function of  $NI/(Vr)^{0.5}$  for the angle of the coil  $\theta = 61^\circ$  and the lengths of the coil  $H = 23, 24, 25$  and  $26$  mm.

The effect of changing the length of the coil ( $H$ ) on spiral distortion coefficient is shown with different values of length of the coil  $H= 23, 24, 25,$  and  $26$  mm, this effect appears in figure (3-16). The calculations show that the coil length  $H = 23\text{mm}$  gives us the lower value of relative spiral distortion coefficient  $D_{sp} * f_o^2$ . The values of relative radial distortion coefficient  $D_{sp} * f_o^2$  increase as the values of the excitation parameter  $NI/(Vr)^{0.5}$  increase.

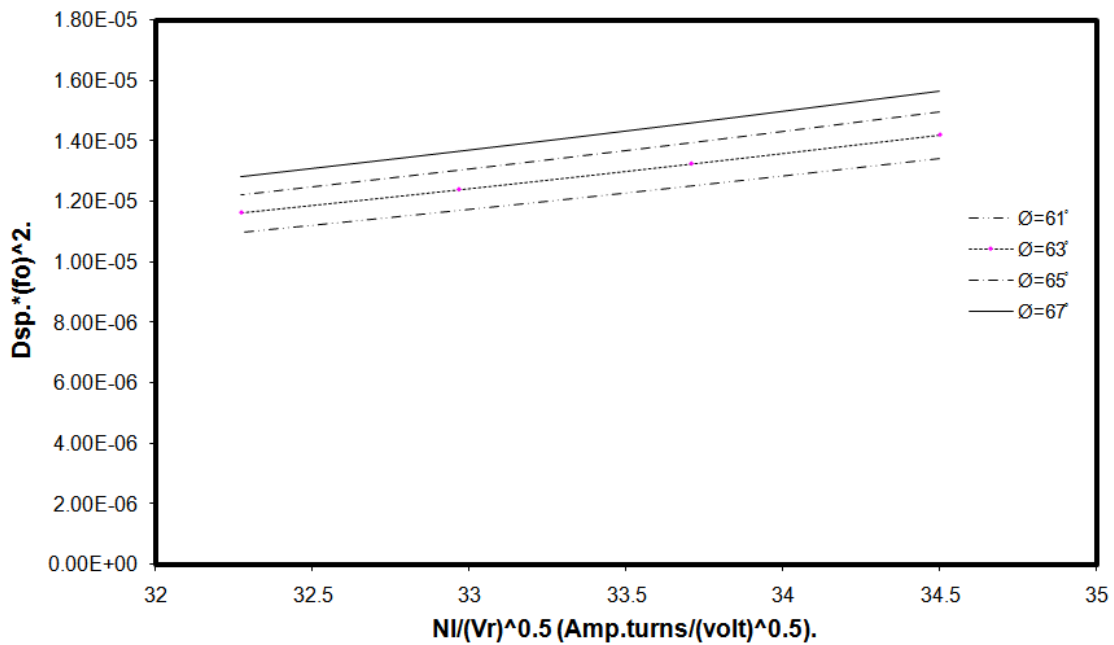


**Figure (3-16): The relative spiral distortion coefficient  $D_{sp} * f_o^2$  as a function of  $NI/(Vr)^{0.5}$  for the length of the coil  $\theta=61^\circ$  and lengths of the coil  $H= 23, 24, 25$  and  $26$  mm.**

The relation between radial and spiral distortion coefficient  $D_{rad} * f_p^2$  and  $D_{sp} * f_p^2$  with the length of the coil is shown in figures (3-17) and (3-18). In these two figures, one can find that the values of radial and spiral distortion coefficient  $D_{rad} * f_p^2$  and  $D_{sp} * f_o^2$  increase as the length of coil increases.

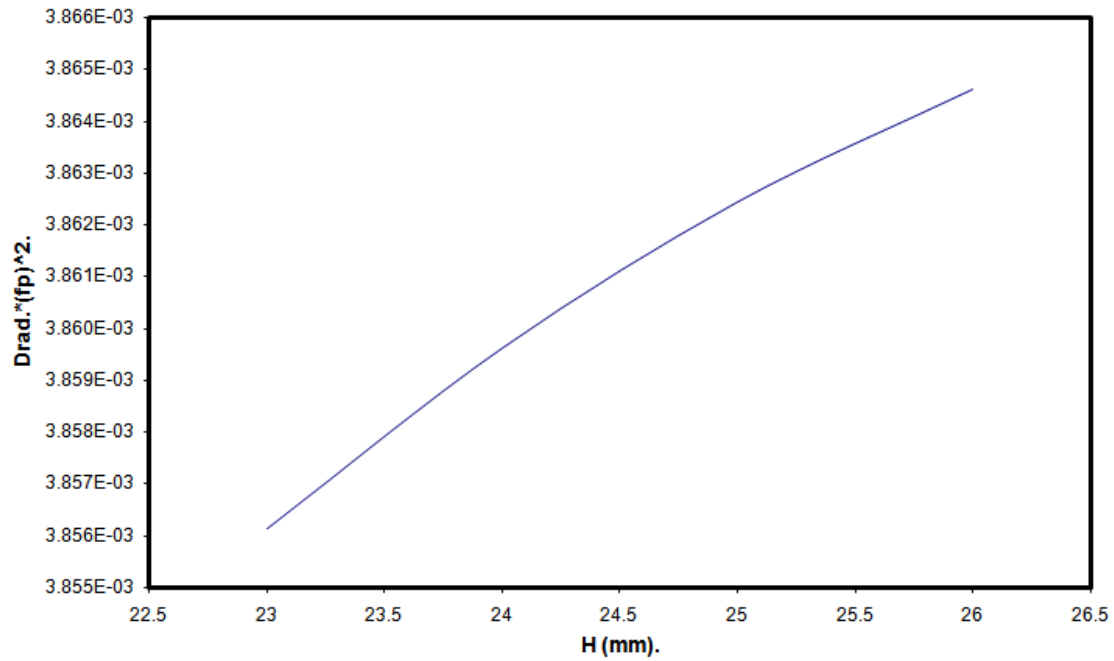


**Figure (3.17):** The relative radial distortion coefficient  $D_{rad} * f_p^2$  as a function of the coil length(H) for the angle of the coil  $\theta=61^\circ$  .

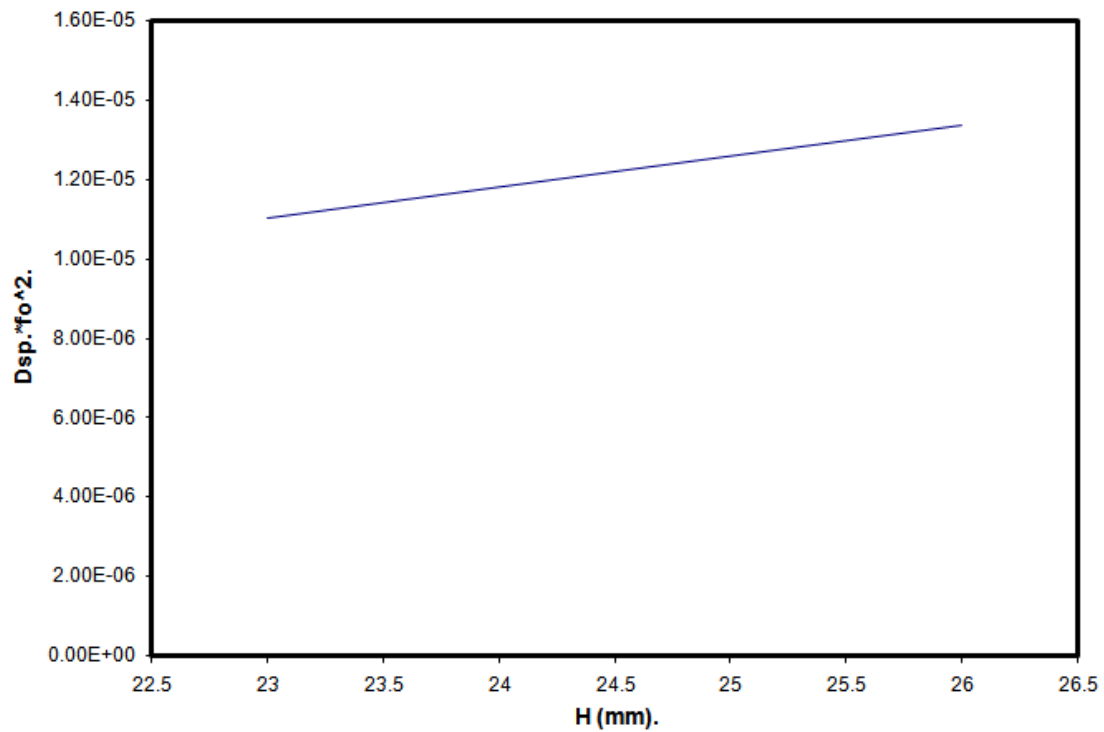


**Figure (3.18):** The relative spiral distortion coefficient  $D_{sp} * f_o^2$  as a function of the coil length (H) for the angle of the coil  $\theta=61^\circ$  .

### 3.4.2 Effects of changing the angle

#### a- Relative spherical and chromatic aberration coefficients

The effect of changing the angles of the coil ( $\theta$ ) on the spherical and chromatic aberration coefficients is investigated and following angles  $\theta = 61^\circ, 63^\circ, 65^\circ,$  and  $67^\circ$  of coil, with coil length  $H = 23\text{mm}$ , are taken into account of aberration coefficients. Figure (3-19) shows the relation between relative spherical aberration coefficient  $C_s/f_o$  and the excitation parameter  $NI/(Vr)^{0.5}$ . This figure shows that  $\theta = 61^\circ$  gives the lower values of spherical aberration coefficient  $C_s/f_o$ . Also the relative spherical aberration coefficient increases with increasing the excitation parameter  $NI/(Vr)^{0.5}$ .

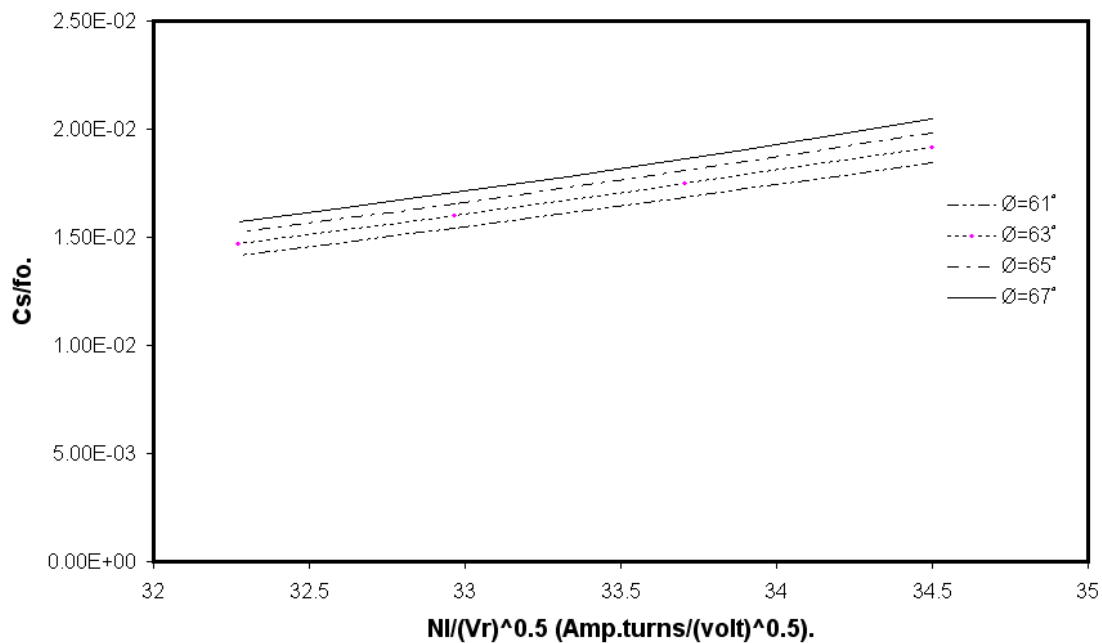
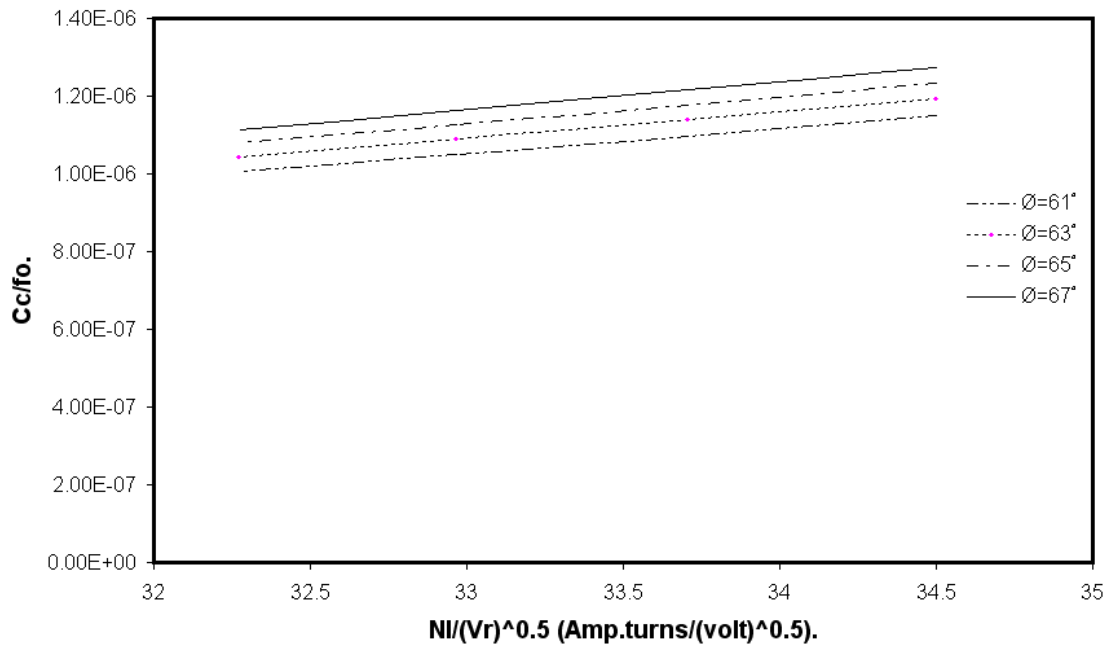


**Figure (3-19):** The relative spherical aberration coefficient  $C_s/f_o$  as a function of  $NI/(Vr)^{0.5}$  for the length of the coil  $H= 23\text{mm}$  and the angle of the coil  $\theta=61^\circ, 63^\circ, 65^\circ,$  and  $67^\circ$ .

Figure (3-20) shows the relation between chromatic aberration coefficient  $C_c/f_o$  and the excitation parameter  $NI/(Vr)^{0.5}$ . From the figure

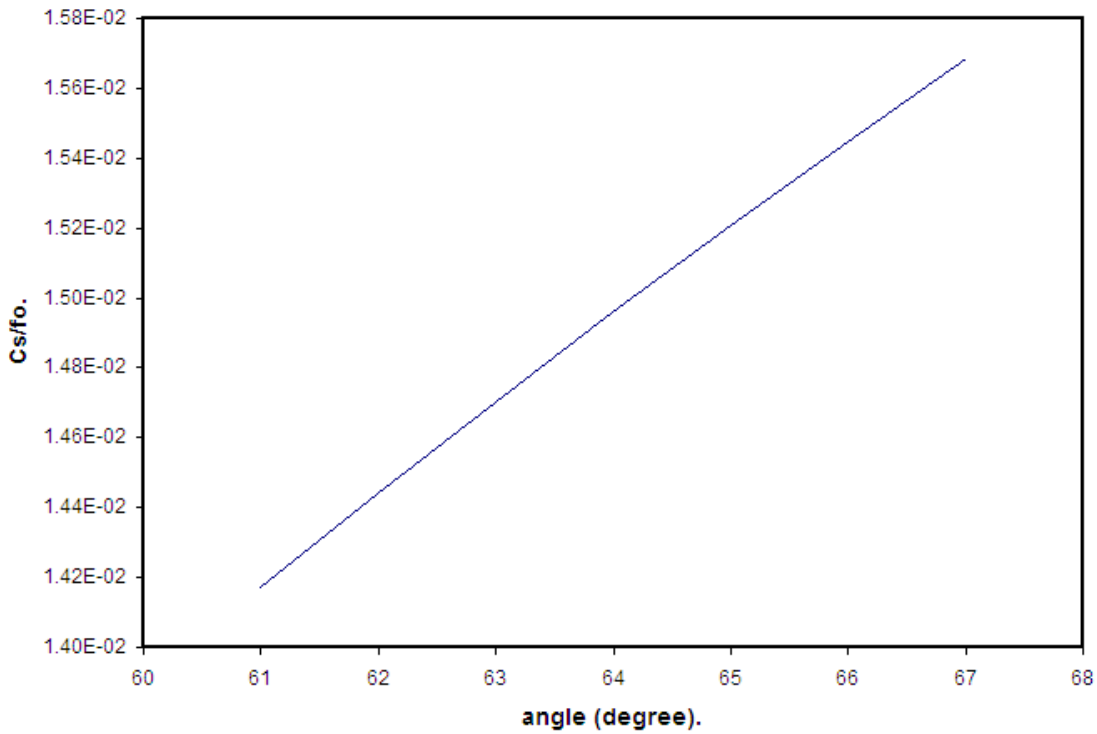


the angle of the coil  $\varnothing = 61^\circ$  gives us the minimum value of chromatic aberration coefficient  $C_c/f_o$ . and the lower values of the excitation parameter  $NI/(Vr)^{0.5}$  give us the best values of the relative chromatic aberration coefficient. From the calculations two parameters can be used to reduce the spherical and chromatic aberration coefficients by selection the best angle and the best value of the ratio of the excitation parameter  $NI/(Vr)^{0.5}$  ( by changing NI and Vr).

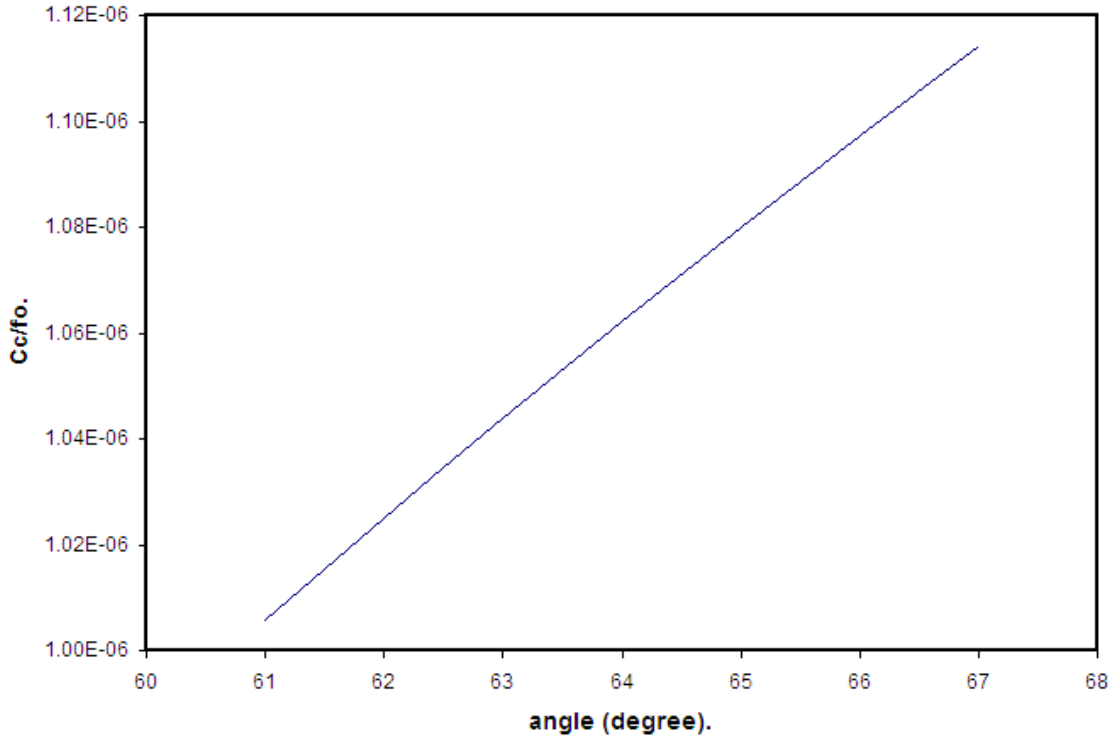


**Figure (3-20):** The relative chromatic aberration coefficient  $C_c/f_o$  as a function of  $NI/(Vr)^{0.5}$  for the length of the coil  $H= 23\text{mm}$  and the angle of the coil  $\varnothing=61^\circ, 63^\circ, 65^\circ, \text{ and } 67^\circ$ .

The relation between spherical and chromatic aberration coefficient  $C_s/f_o$  and  $C_c/f_o$  with the angle of the coil ( $\theta$ ) is shown in figures (3-21) and (3-22), respectively at the excitation parameter  $NI/(V_T)^{0.5} = 32.27$  Amp. turns/(volt)<sup>0.5</sup>. Both cases have the same behavior, where the spherical and chromatic aberration coefficient  $C_s/f_o$  and  $C_c/f_o$  decrease as the angle of the coil decreases.



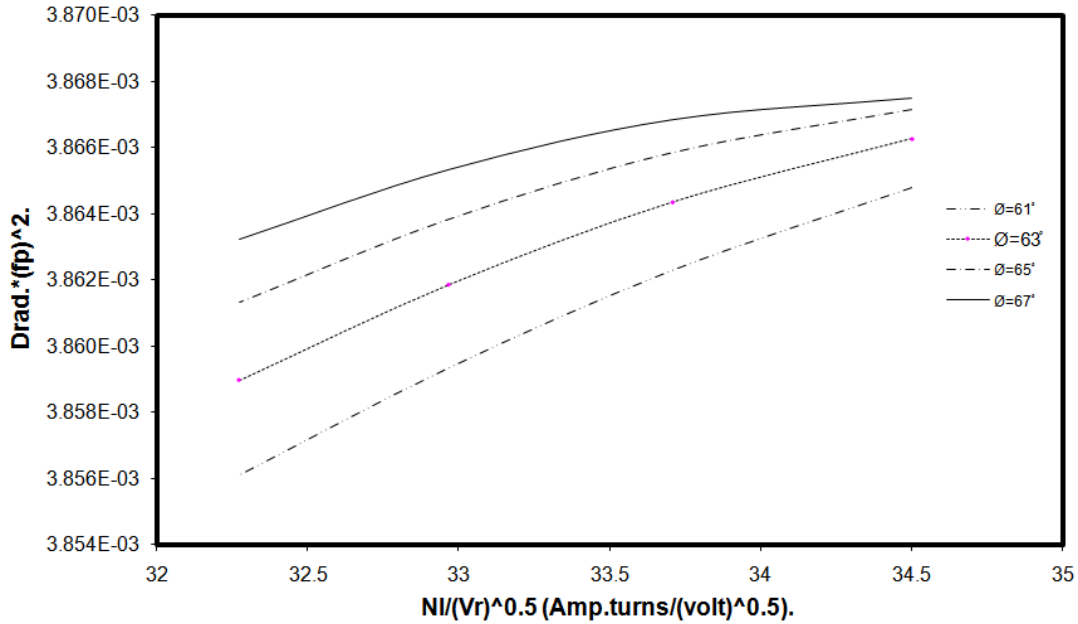
**Figure (3-21): The relative spherical aberration coefficient  $C_s/f_o$  as a function of the angle of the coil ( $\theta$ ) for the length of the coil**



**Figure (3.22):** *The relative chromatic aberration coefficient  $C_c/f_o$  as a function of the angle of coil ( $\theta$ ) for the length of the coil  $H=23$  mm.*

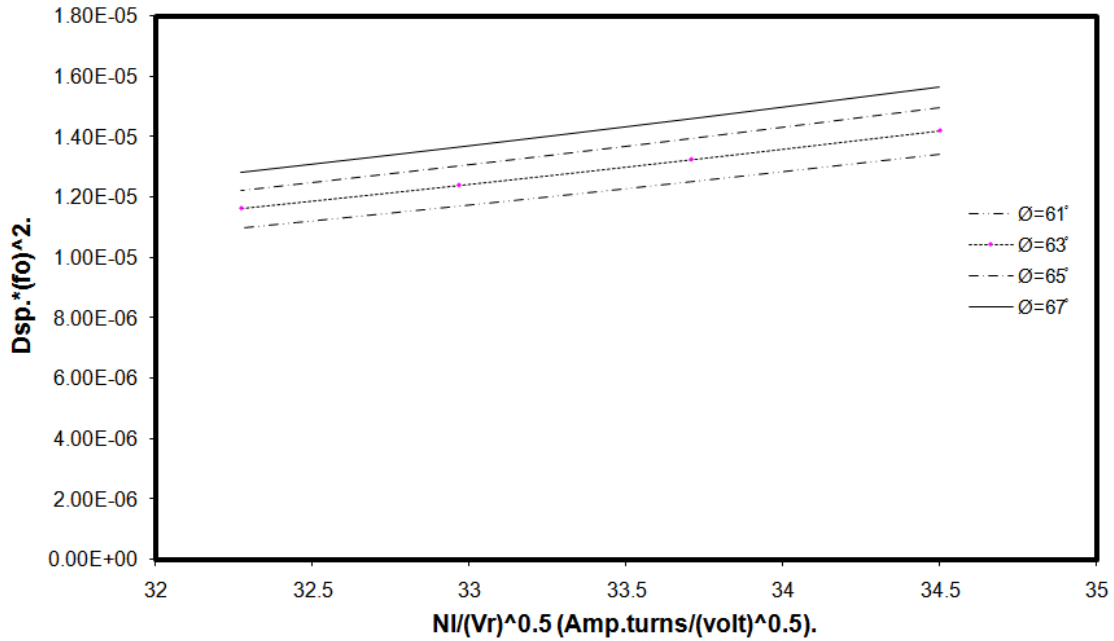
### **b- Relative radial and spiral distortion coefficients**

Different angles,  $\theta=61^\circ$ ,  $63^\circ$ ,  $65^\circ$ , and  $67^\circ$ , of the coil are taken in computation the radial and spiral distortion coefficients. Figure (3-23) explain the results of these calculations. In this figure, the values of the radial distortion coefficients  $D_{rad} * f_p^2$  decreases as the excitation parameter  $NI/(Vr)^{0.5}$  decreases. Also, the angle of the coil  $\theta = 61^\circ$  and lower values of the excitation parameter  $NI/(Vr)^{0.5}$  gives us the lower value of relative radial distortion coefficient  $D_{rad} * f_p^2$ .



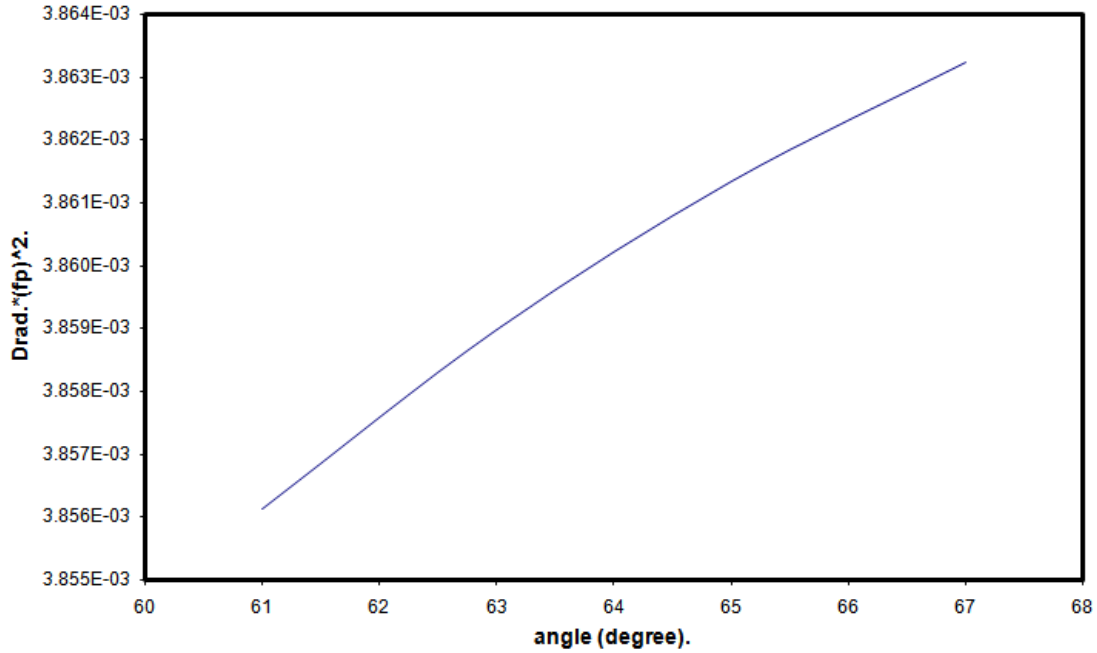
**Figure (3-23):** The relative radial distortion coefficient  $D_{rad} * f_p^2$  as a function of  $NI/(Vr)^{0.5}$  for the length of the coil  $H= 23mm$  and the angle of the coil  $\theta=61^\circ, 63^\circ, 65^\circ, \text{ and } 67^\circ$ .

Figure (3-24) explain the relation between the spiral distortion coefficients with the excitation parameter  $NI/(Vr)^{0.5}$ . From the calculations of four angles one can find that the minimum values of relative spiral distortion coefficient  $D_{sp} * f_o^2$  occur at angle  $\theta = 61^\circ$  and the lower value of the excitation parameter  $NI/(Vr)^{0.5}$ .



**Figure (3-24):** The relative spiral distortion coefficient  $D_{sp} * f_o^2$  as a function of  $NI/(Vr)^{0.5}$  for the length of the coil  $H= 23mm$  and the angle of the coil  $\theta=61^\circ, 63^\circ, 65^\circ, \text{ and } 67^\circ$ .

The relation between the radial and spiral aberration coefficients  $D_{rad} * f_p^2$  and  $D_{sp} * f_o^2$  with the angle of coil ( $\theta$ ) is shown in figures (3-25) and (3-26), respectively with the excitation parameter  $NI/(Vr)^{0.5} = 32.27$  Amp. turns/(volt)<sup>0.5</sup>. In both cases the radial and spiral aberration coefficient  $D_{rad} * f_p^2$  and  $D_{sp} * f_o^2$  increases as the angle increases.



**Figure (3.25):** The relative radial distortion coefficient  $D_{rad} \cdot f_p^2$  as a function of the angle of the coil ( $\theta$ ) for the length of the coil  $H=23$  mm.

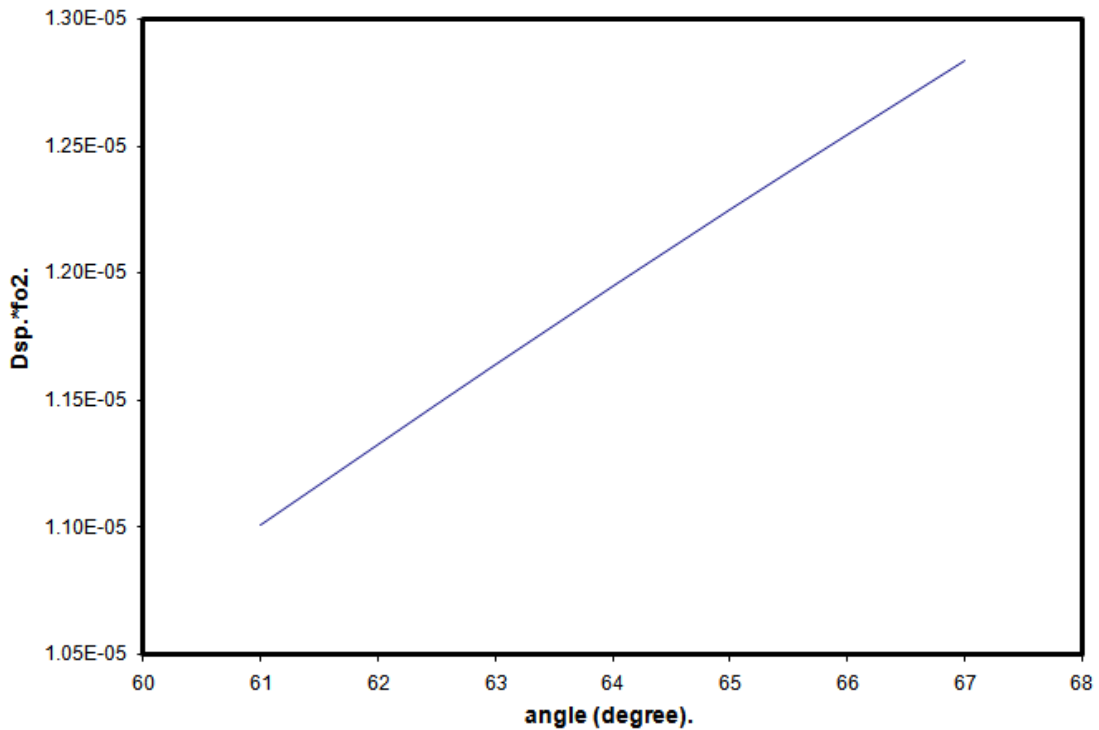


**Figure (3.26):** The relative spiral distortion coefficient  $D_{sp} \cdot f_o^2$  as a function of the angle of the coil ( $\theta$ ) for the length of the coil  $H=23$  mm.

### 3.5 Zero Magnification Condition

#### 3.5.1 Effects of changing the length

##### a-Relative spherical and chromatic aberration coefficients

The variation of the length of the coil has been studied to find the optimum length of the coil which gives us the minimum values of spherical and chromatic aberration coefficients under zero magnification condition. The calculations for different values of the length of the coil,  $H = 23, 24, 25,$  and  $26\text{mm}$ , are made for the angle of the coil  $\theta = 61^\circ$ . Figure (3-27) shows the results of spherical aberration coefficients. In this figure one can find that the length of the coil  $H = 23\text{mm}$  gives the lower values of spherical aberration coefficient  $C_s/f_o$  at lower value of excitation parameter  $NI/(V_r)^{0.5}$ .

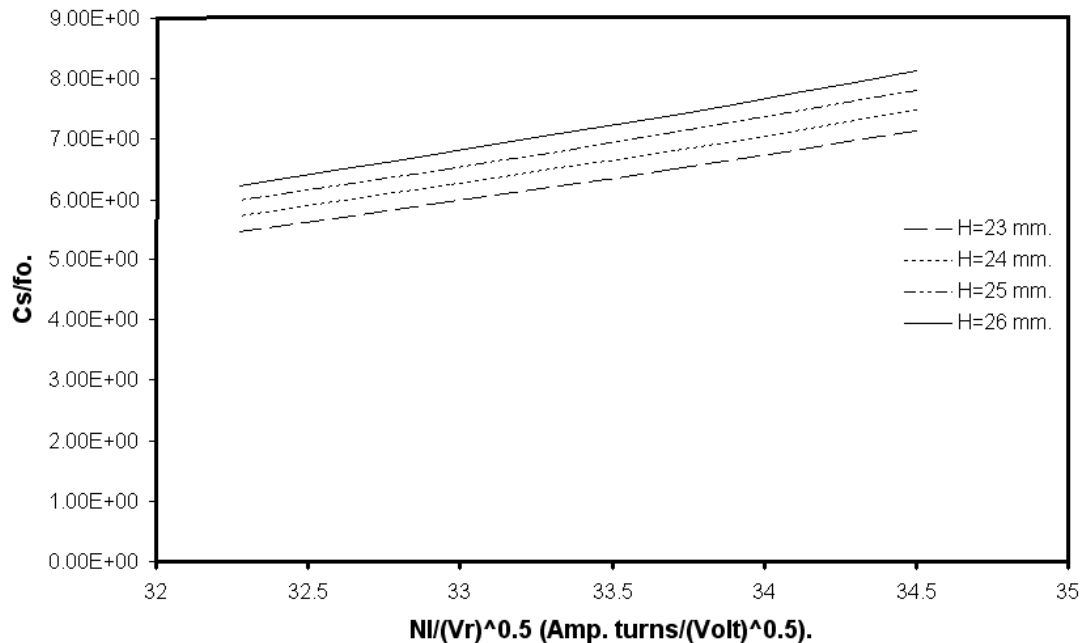


**Figure (3-27):** The relative spherical aberration coefficient  $C_s/f_o$  as a function of  $NI/(V_r)^{0.5}$  for the angle of the coil  $\theta=61^\circ$  and the length of the coil  $H= 23, 24, 25$  and  $26$  mm.

The effect of variation of the coil length on the relative chromatic aberration coefficient is shown in figure (3-28). One finds that at the length of the coil  $H = 23\text{mm}$  gives the best value of spherical aberration coefficient  $C_c/f_o$  at lower value of excitation parameter  $NI/(Vr)^{0.5}$ . One can note that the relation from the figure is linear between  $C_c/f_o$  and the length of the coil  $H$ .

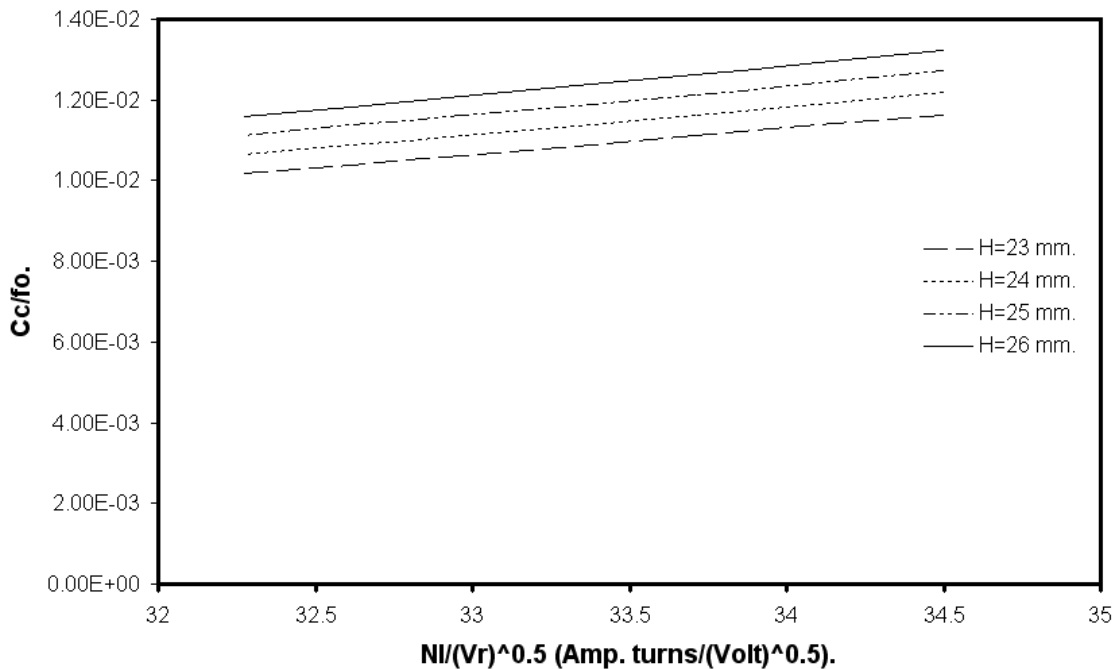


**Figure (3-28): The relative chromatic aberration coefficient  $C_c/f_o$  as a function of  $NI/(Vr)^{0.5}$  for the angle of the coil  $\theta=61^\circ$  and the length of the coil  $H= 23, 24, 25$  and  $26$  mm.**

The relation between spherical and chromatic aberration coefficients  $C_s/f_o$  and  $C_c/f_o$  with the length of the coil ( $H$ ) is shown in the figures (3-29) and (3-30), respectively at constant value of the excitation parameter  $NI/(Vr)^{0.5} = 32.72$  Amp. turns/(volt)<sup>0.5</sup>. The values of spherical and chromatic aberration coefficients  $C_s/f_o$  and  $C_c/f_o$  increase when the



length of the coil increases and the length of the coil  $H = 23\text{mm}$  gives us the lower values.

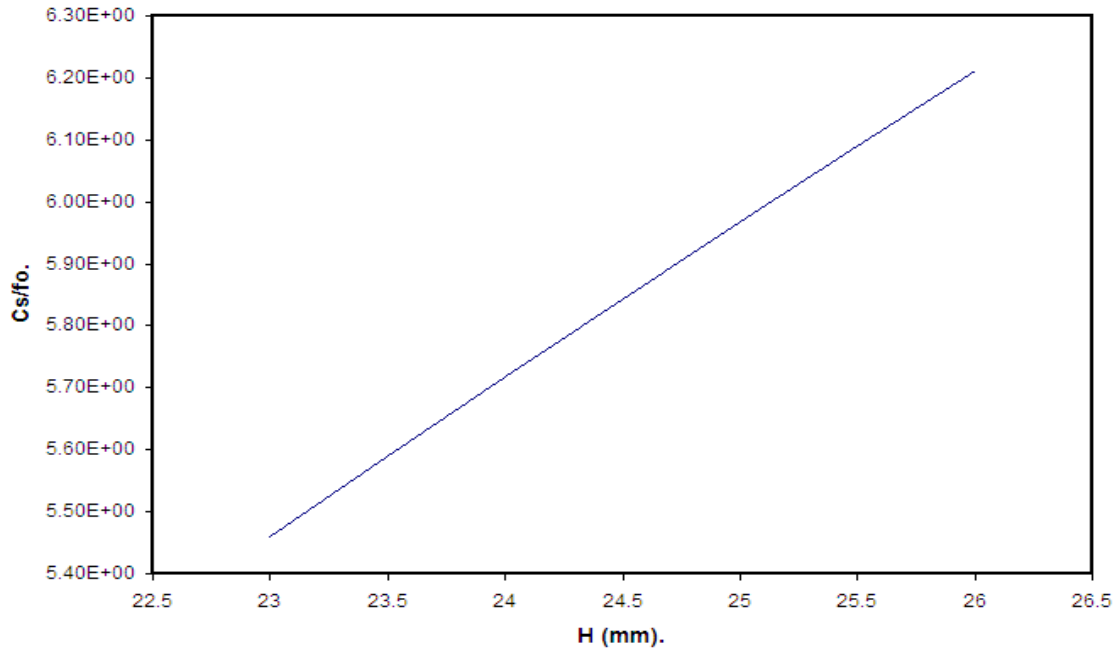


**Figure (3-29):** The relative spherical aberration coefficient  $C_s/f_o$  as a function of the coil length ( $H$ ) for the angle of the coil  $\theta=61^\circ$ .

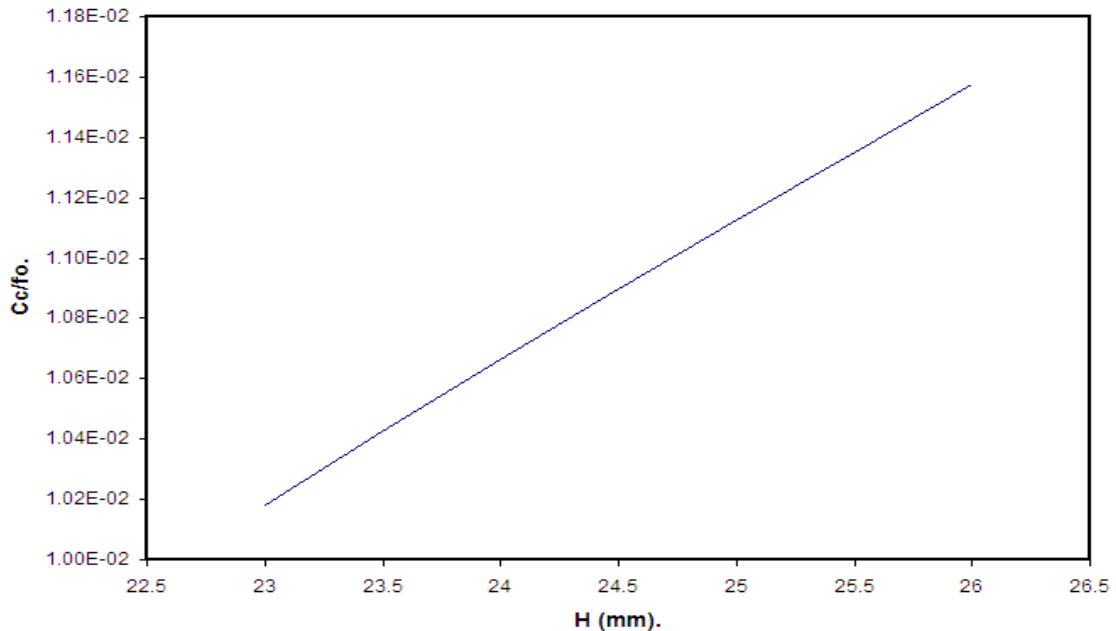


**Figure (3-30):** The relative chromatic aberration coefficient  $C_c/f_o$  as a function of the coil length ( $H$ ) for the angle of the coil  $\theta=61^\circ$ .

## b- Relative radial and spiral distortion coefficients

The different values of length of the coil,  $H= 23, 24, 25,$  and  $26$  mm with the angle of the coil  $\vartheta=61^\circ$ , are studied to find the optimum length which give us the best values of radial and spiral distortion coefficient  $D_{rad} * f_p^2$  and  $D_{sp} * f_o^2$ . The results of radial distortion are shown in figure (3-31). In this figure, the length of the coil  $H = 23$ mm represent the optimum length. The effect of changing the length of the coil on spiral distortion is shown in figure (3-32). In this figure it appears that the length of the coil  $H = 23$ mm gives the best result. Both radial and spiral distortion aberration coefficients have the same relation with the length of the coil, where the relative radial and spiral distortion coefficients increase as the length of the coil increase and this relation appears in figures (3-33) and (3-34).

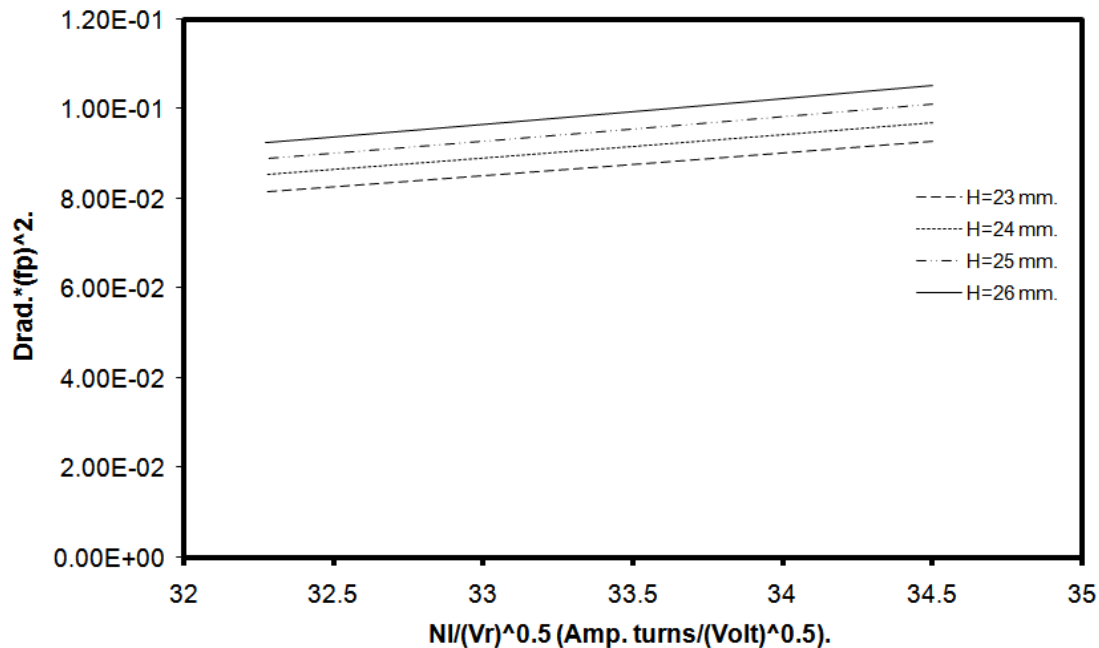


**Figure (3-31):** The relative radial distortion coefficient  $D_{rad} * f_p^2$  as a function of  $NI/(Vr)^{0.5}$  for the angle of the coil  $\vartheta=61^\circ$  and the length of the coil  $H= 23, 24, 25$  and  $26$  mm.

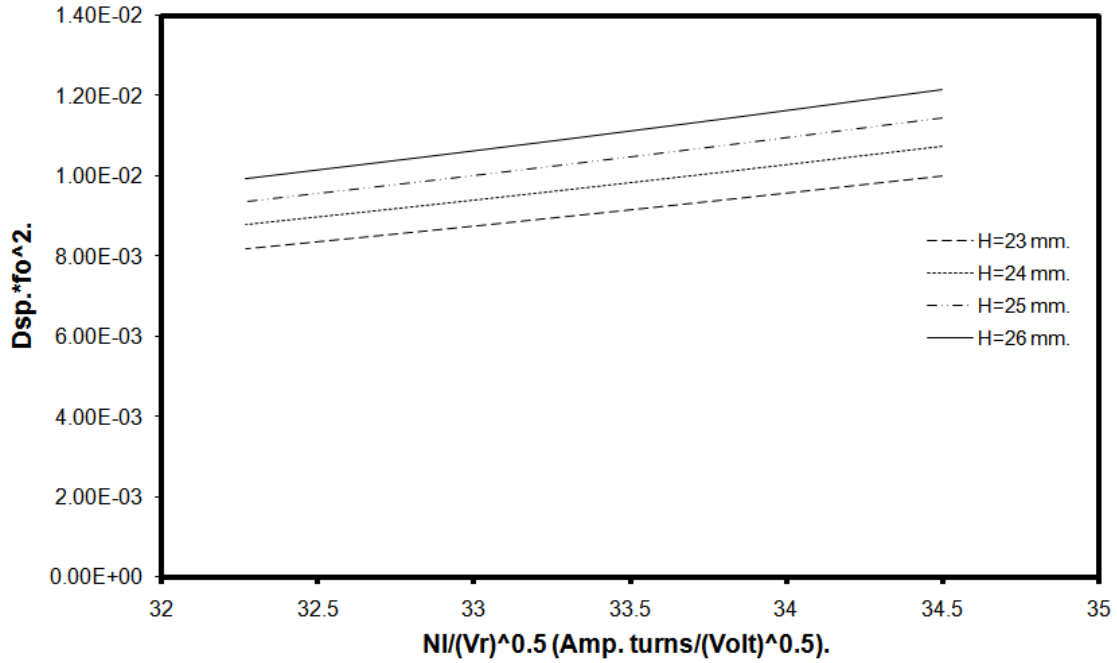


**Figure (3-32):** The relative spiral distortion coefficient  $D_{sp} * f_o^2$  as a function of  $NI/(Vr)^{0.5}$  for the angle of the coil  $\theta=61^\circ$  and the length of the coil  $H= 23, 24, 25$  and  $26$  mm.

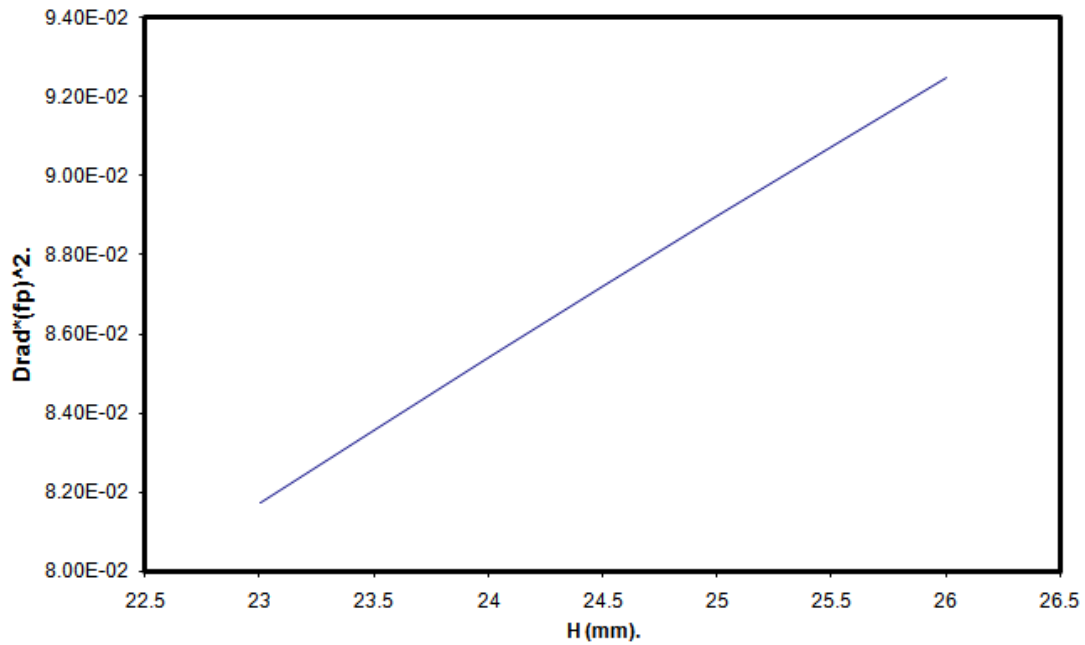


**Figure (3-33):** The relative radial distortion coefficient  $D_{rad} * f_p^2$  as a function of the coil length ( $H$ ) for the angle of the coil  $\theta=61^\circ$ .

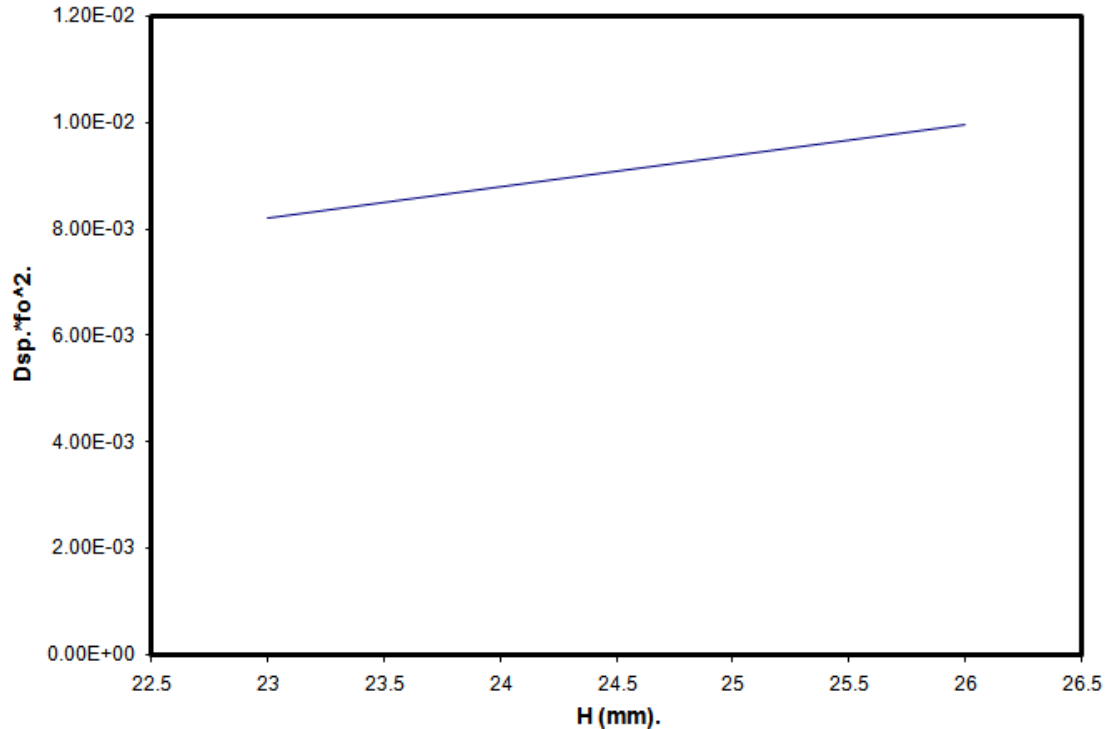
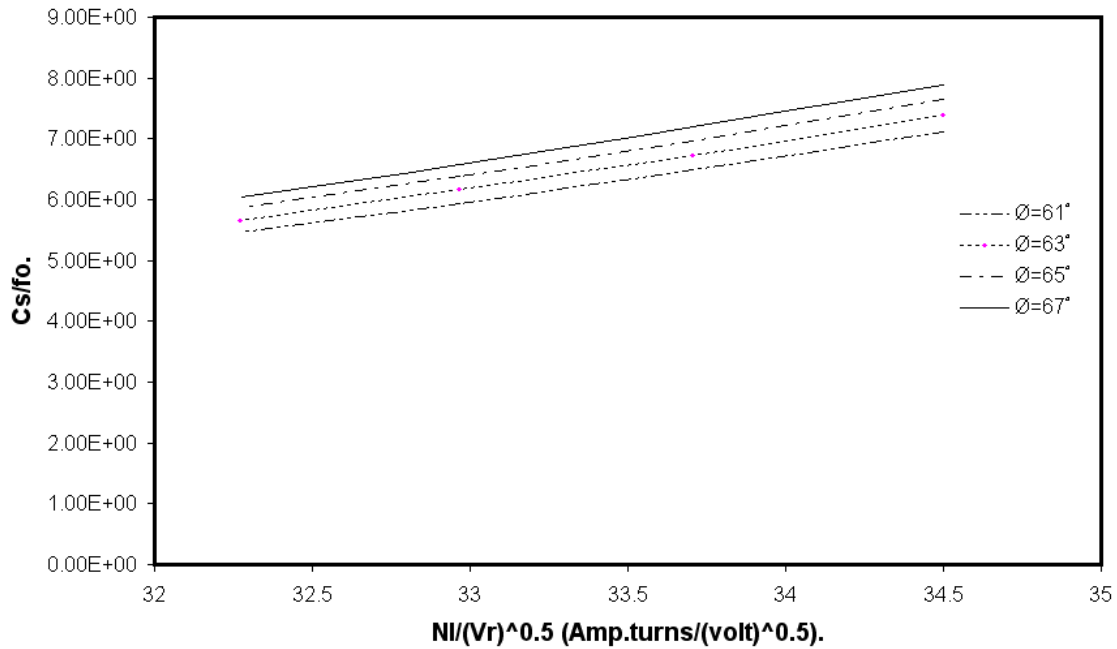


*Figure (3.34): The relative spiral distortion coefficient  $D_{sp} * f_o^2$  as a function of the coil length (H) for the angle of the coil  $\theta=61^\circ$ .*

### 3.5.2 Effects of changing the angle

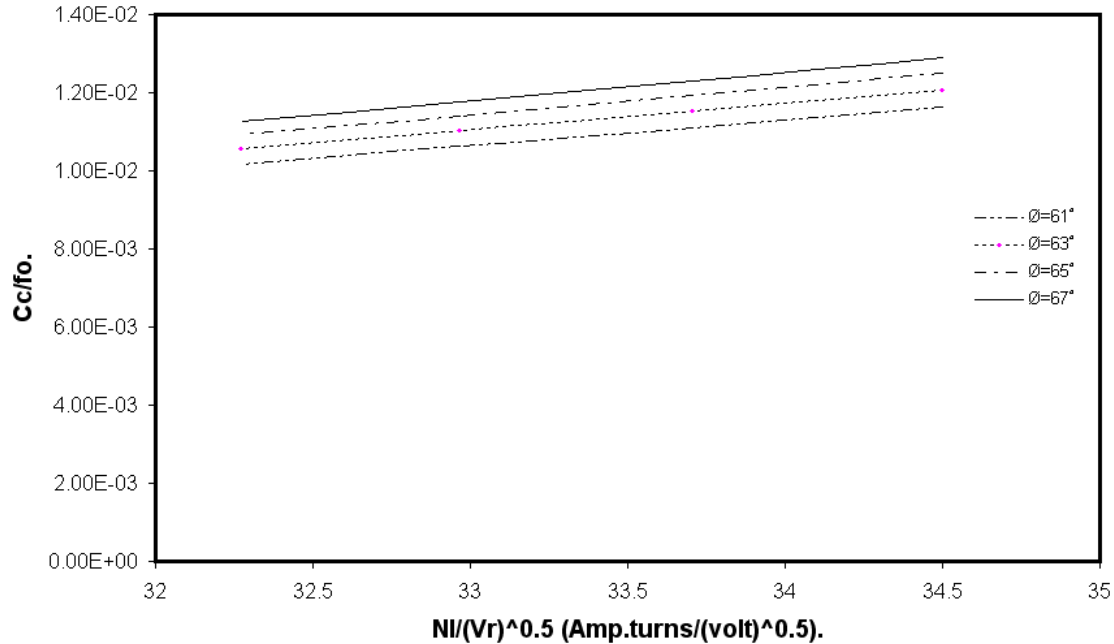
#### a- Relative spherical and chromatic aberration coefficients

Different angles of coil,  $\theta = 61^\circ, 63^\circ, 65^\circ$  and  $67^\circ$  with constant length of coil  $H = 23\text{mm}$ , are used in calculations to study the effect of changing the angle of the coil on both spherical and chromatic aberration coefficients. Figure (3-35) shows the relation between spherical aberration coefficient  $C_s / f_o$  and the excitation parameter  $NI/(Vr)^{0.5}$ . In this figure, the angle of the coil  $\theta = 61^\circ$  give the lower value of aberration coefficients. From the figure one can also see that the quotient spherical aberration coefficient  $C_s / f_o$  increases when the ratio of the excitation parameter  $NI/(Vr)^{0.5}$  increases.



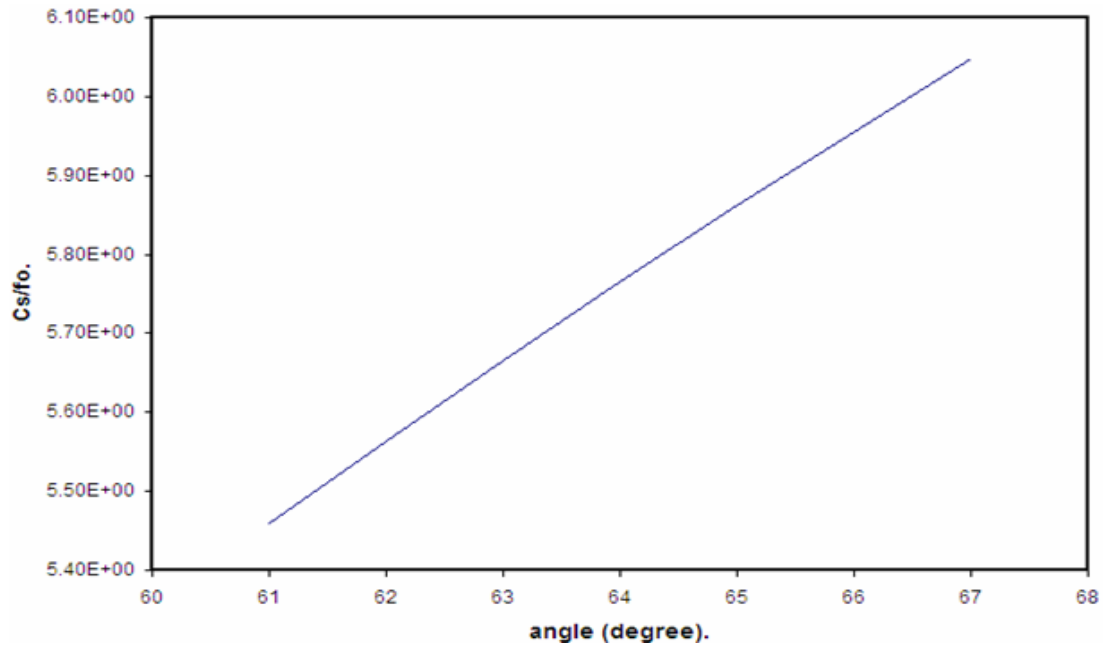
**Figure (3-35):** The relative spherical aberration coefficient  $C_s/f_o$  as a function of  $NI/(Vr)^{0.5}$  for the length of the coil  $H= 23\text{mm}$  and the angle of the coil  $\varnothing=61^\circ, 63^\circ, 65^\circ, \text{ and } 67^\circ$ .

Figure (3-36) shows the relation between chromatic aberration coefficients  $C_c/f_o$  and  $NI/(Vr)^{0.5}$ . In this figure, the angle of the coil  $\varnothing = 61^\circ$  give us the best value of the chromatic aberration coefficients  $C_c/f_o$  at the lower value of excitation parameter  $NI/(Vr)^{0.5}$ . The value of relative chromatic aberration coefficients has the same behavior as relative spherical aberration coefficients in figure (3-35). At the smaller values of the excitation parameter  $NI/(Vr)^{0.5}$  one can find the minimum values of both spherical and chromatic aberrations and by choosing the values of  $NI$  and  $Vr$  one can keep aberration coefficients small.

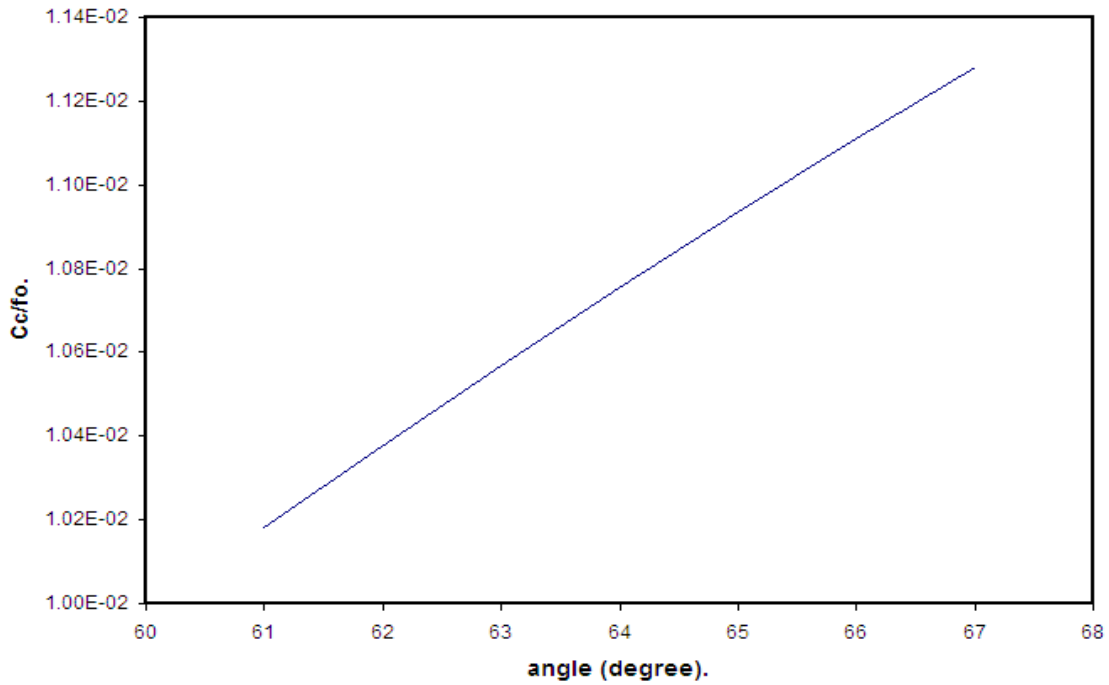


**Figure (3-36):** The relative chromatic aberration coefficient  $C_c/f_o$  as a function of  $NI/(Vr)^{0.5}$  for the length of the coil  $H= 23\text{mm}$  and the angle of the coil  $\theta=61^\circ, 63^\circ, 65^\circ, \text{ and } 67^\circ$ .

The relation between the spherical and chromatic aberration coefficients  $C_s/f_o$  and  $C_c/f_o$  with the angle of coil ( $\theta$ ) is shown in figures (3-37) and (3-38), respectively with the excitation parameter  $NI/(Vr)^{0.5} = 32.27 \text{ Amp. turns}/(\text{volt})^{0.5}$ . In both cases the spherical and chromatic aberration coefficients  $C_s/f_o$  and  $C_c/f_o$  values decreases as value of the angle of the coil  $\theta$  decreases. The optimum values of the spherical and chromatic aberration coefficients  $C_s/f_o$  and  $C_c/f_o$  at the angle of the coil  $\theta = 61^\circ$  and lower value of excitation parameter  $NI/(Vr)^{0.5}$ .



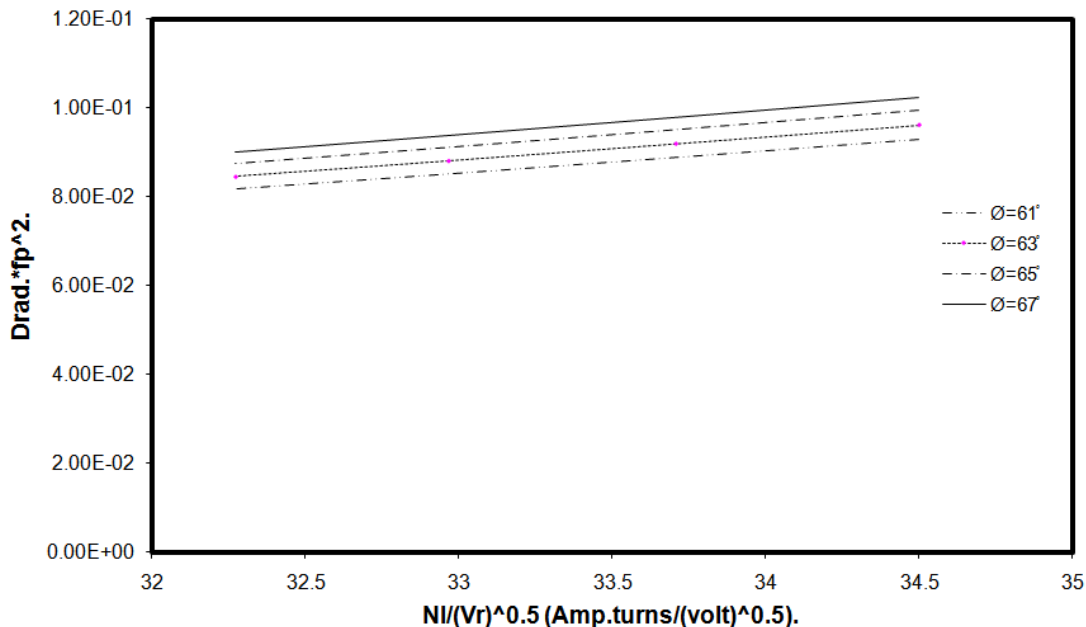
***Figure (3-37): The relative spherical aberration coefficient  $C_s/f_o$  as a function of the angle of the coil ( $\theta$ ) for the length of the coil  $H=23\text{mm}$ .***



***Figure (3-38): The relative chromatic aberration coefficient  $C_c/f_o$  as a function of the angle of the coil ( $\theta$ ) for the length of the coil  $H=23\text{ mm}$ .***

## b- Relative radial and spiral distortion coefficients

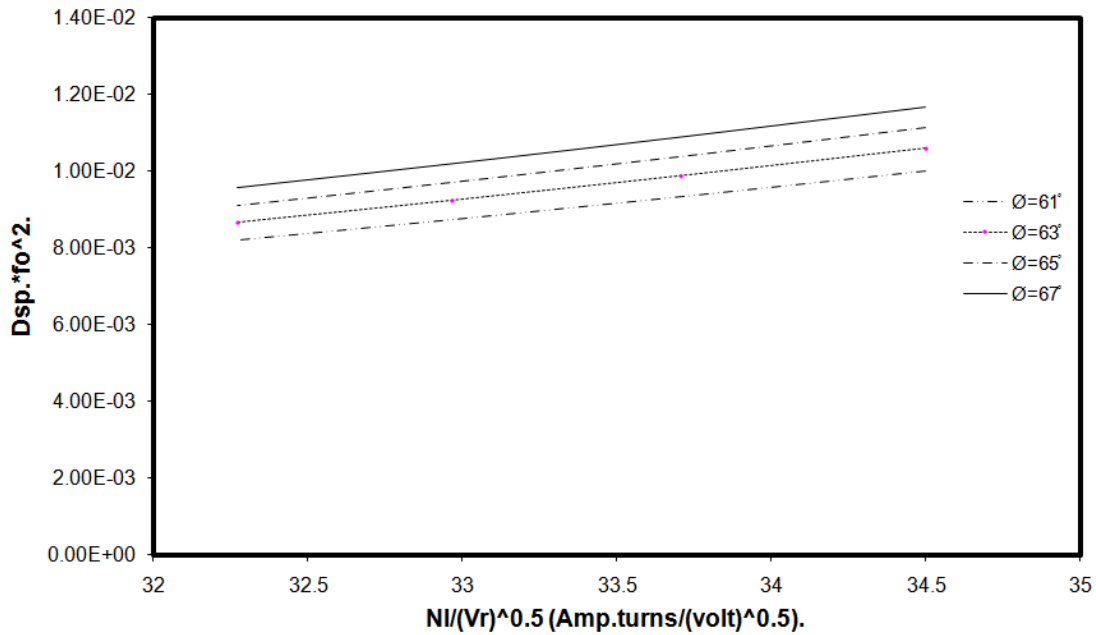
The different angles of coil,  $\theta = 61^\circ, 63^\circ, 65^\circ$  and  $67^\circ$  with constant length of coil  $H = 23\text{mm}$ , are used in calculations to study the effect of changing of the angle of the coil on both radial and spiral distortion coefficients. Figure (3-39) shows the relation between radial distortion coefficients  $D_{\text{rad}} * f_p^2$  and  $NI/(Vr)^{0.5}$ . In this figure, the angle of the coil  $\theta = 61^\circ$  gives the optimum value of radial distortion coefficients  $D_{\text{rad}} * f_p^2$ . Also the ratio of the radial distortion coefficients  $D_{\text{rad}} * f_p^2$  increases as the excitation parameter  $NI/(Vr)^{0.5}$  increases.



**Figure (3-39):** The relative radial distortion coefficient  $D_{\text{rad}} * f_p^2$  as a function of  $NI/(Vr)^{0.5}$  for the length of the coil  $H = 23\text{mm}$  and the angle of the coil  $\theta = 61^\circ, 63^\circ, 65^\circ$ , and  $67^\circ$ .

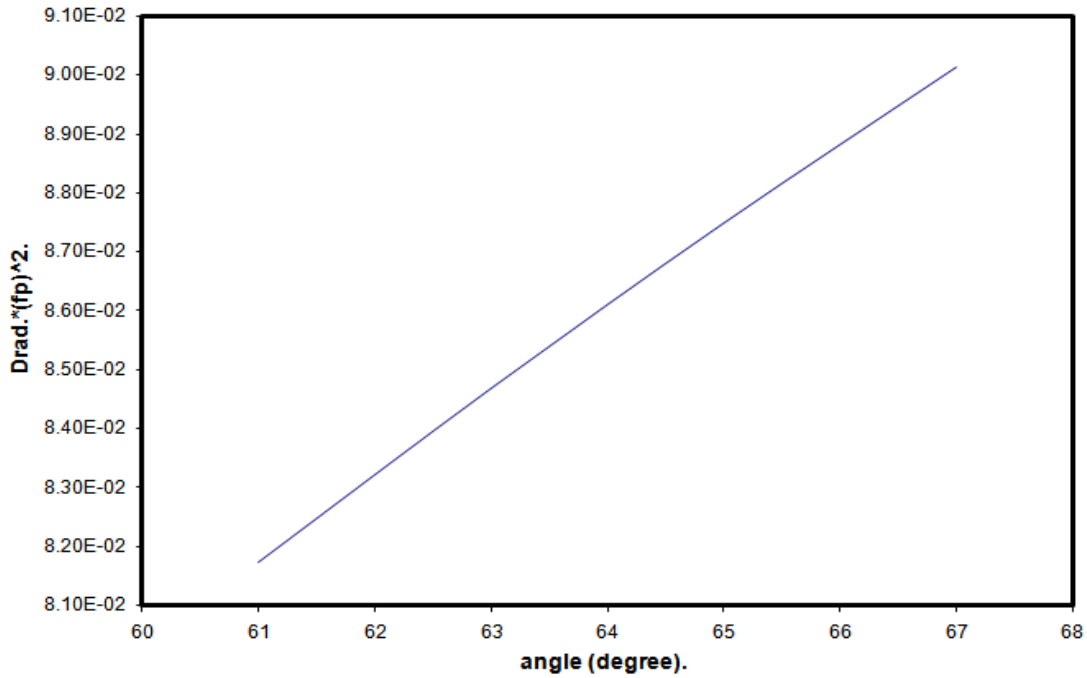


Figure (3-40) shows the relation between spiral distortion coefficients  $D_{sp} * f_o^2$  and  $NI/(Vr)^{0.5}$  for different angles of coil  $\varnothing = 61^\circ, 63^\circ, 65^\circ$  and  $67^\circ$ , respectively. In this figure, the values of spiral distortion coefficients  $D_{sp} * f_o^2$  are reduced when the excitation parameter  $NI/(Vr)^{0.5}$  decreases and the lower value of the  $D_{sp} * f_o^2$  occur at the angle of the coil  $\varnothing = 61^\circ$ .



**Figure (3-40): The relative spiral distortion coefficient  $D_{sp} * f_o^2$  as a function of  $NI/(Vr)^{0.5}$  for the length of the coil  $H= 23mm$  and the angle of the coil  $\varnothing=61^\circ, 63^\circ, 65^\circ, \text{ and } 67^\circ$ .**

The relation between the radial and spiral distortion coefficient  $D_{rad} * f_p^2$  and  $D_{sp} * f_o^2$  with the angles of coil ( $\varnothing$ ) is shown in figures (3-41) and (3-42), respectively at the excitation parameter  $NI/(Vr)^{0.5} = 32.27$  Amp. turns/(volt)<sup>0.5</sup>. Both cases have the same behavior, where the radial and spiral distortion coefficient  $D_{rad} * f_p^2$  and  $D_{sp} * f_o^2$  are increases as the angle of the coil  $\varnothing$  increases.



**Figure (3.41):** The relative radial distortion coefficient  $D_{rad} * f_p^2$  as a function of the angle of the coil ( $\theta$ ) for length of the coil  $H=23$  mm.

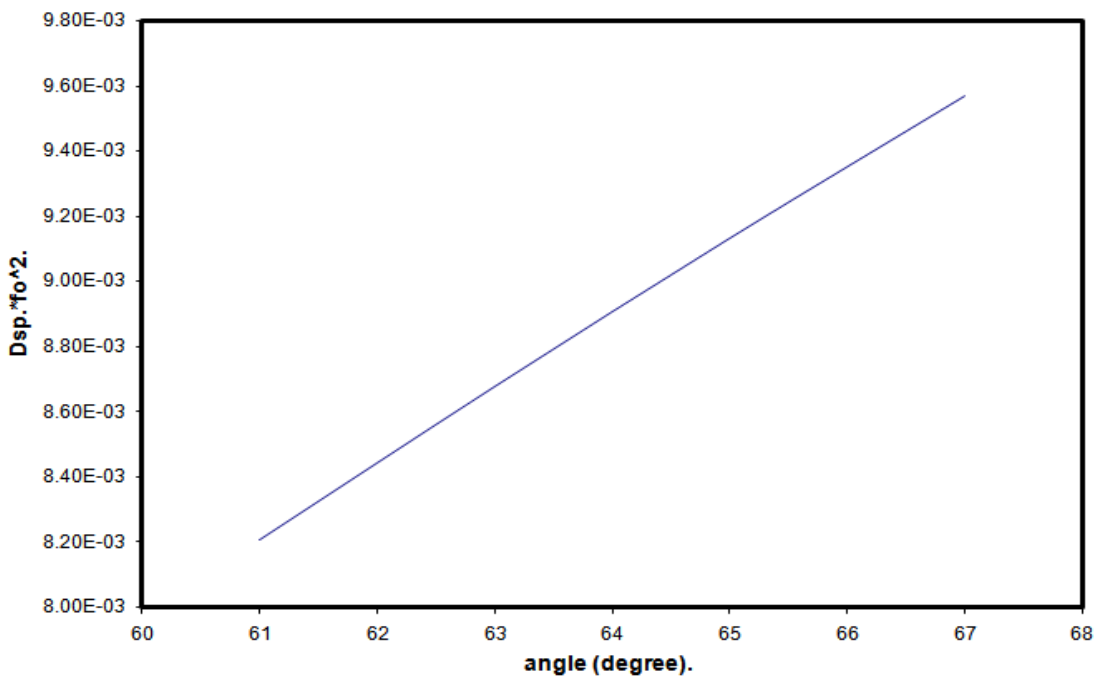


**Figure (3-42):** The relative spiral distortion coefficient  $D_{sp} * f_o^2$  as a function of the angle of the coil ( $\theta$ ) for length of the coil  $H=23$  mm.

### 3.6 pole pieces Reconstruction

The pole piece shape is found by using the reconstruction method with aid of equation (2-12) and figure (3-43) shows the shape of the pole piece for the angle of the coil  $\theta = 61^\circ$  and the length of the coil  $H = 23\text{mm}$ . The parameters (L) in the figure represent the length of the system field.

In the figure the lower part represent the pole piece shape of the lens and the upper parts represent the pole piece shape of the deflector.

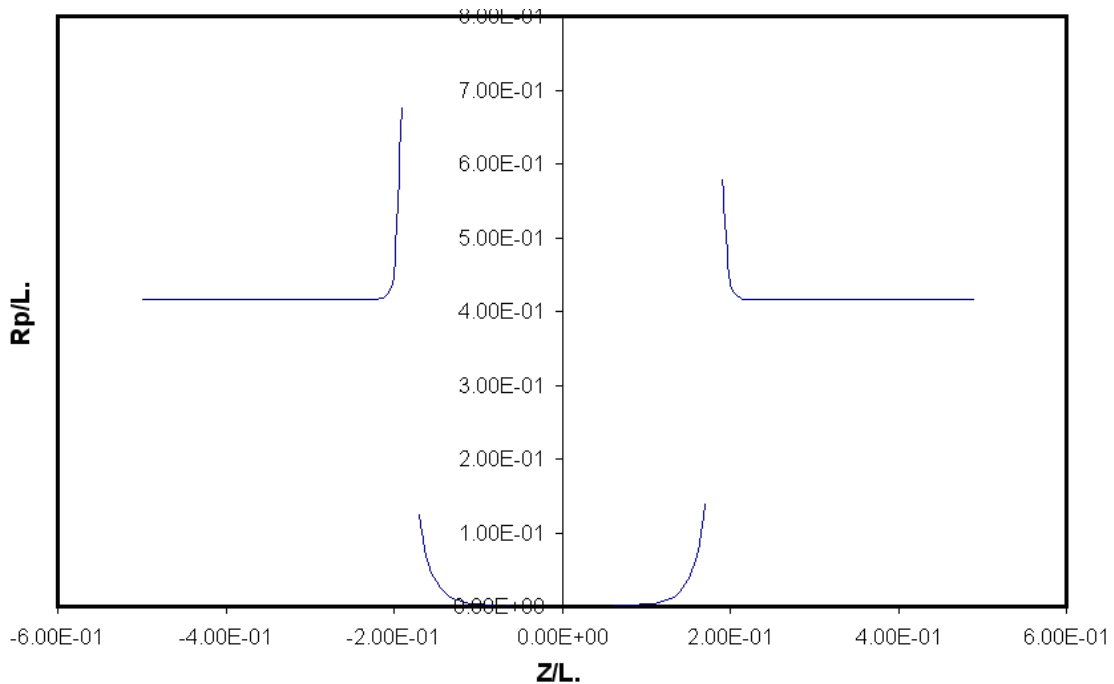
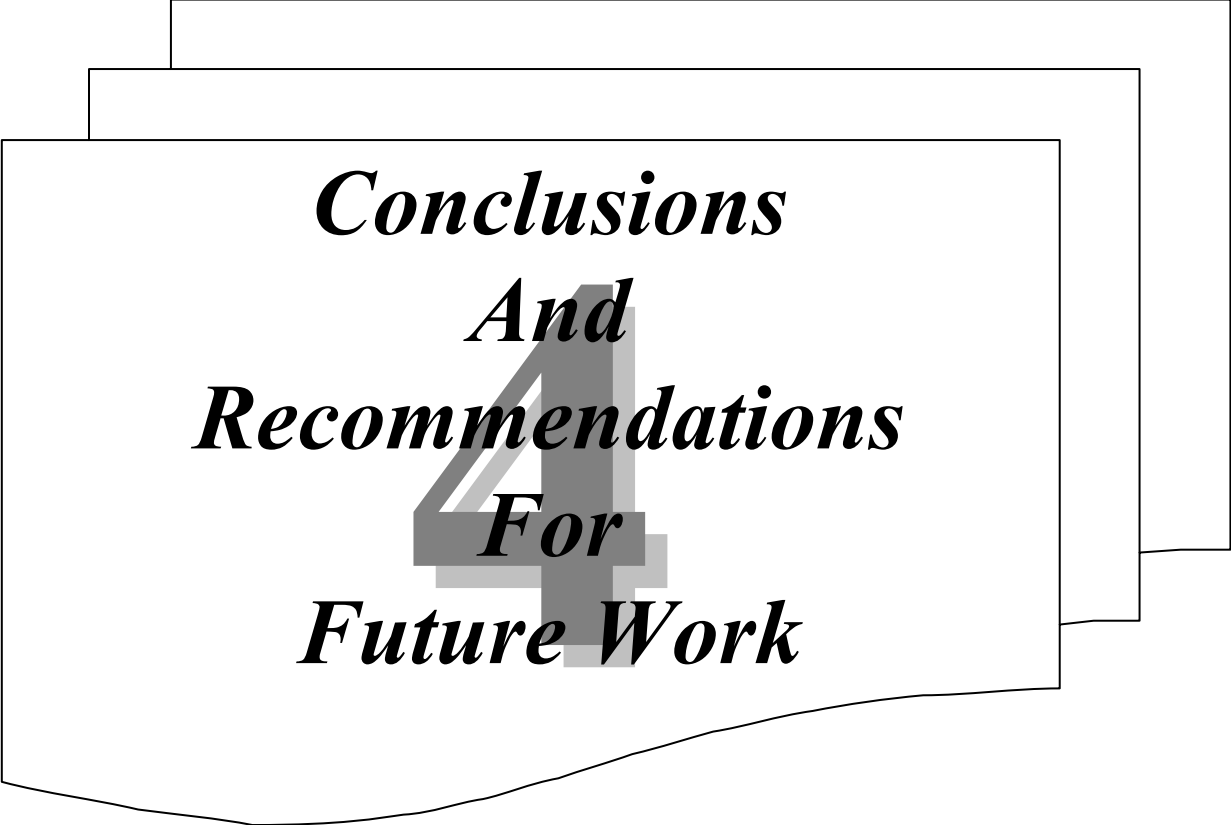


**Figure (3.43):** The pole piece shape when the length of the coil  $H=23\text{ mm}$  and the angle of the coil  $\theta=61^\circ$ .

*Chapter*  
*Four*



*Conclusions*  
*And*  
*Recommendations*  
*For*  
*Future Work*

## *Chapter Four*

### Conclusions and Suggestions for Future Work

#### **4.1 Conclusions**

From the results one can conclude that:-

- 1 - The length and angle are inversely proportionate with the four coefficient of aberrations in the cases of zero and infinite magnification conditions. therefore the smaller size coil of the deflection has improved the values of aberration.
- 2 - The relationship between the four coefficient of aberrations and length and angle of the coil is inversely proportional in the cases of zero and infinite magnification conditions, therefore, provides us with the possibility of operating the system with high efficiency in different operation conditions of the system.
- 3 - The field is increasing as the values of angle and length of the coil increases.
- 4- The aberration coefficients are directly proportional to the field, also the field is increasing when the length and angle of the coil increase therefore the aberration coefficients are increasing when the length and angle of the coil increase.

#### **4.2 Recommendations for Future Work**

There are following topic put forward for future investigations

- (a)** We recommend using different types of axial magnetic field model.
- (b)** We recommend using different types of coils as sources of magnetic field.



***References***

## *References*

**Alamir A. S. A. (2003)**

*Spiral distortion of magnetic lenses with fields of the form  $\mathcal{B}(z) \propto z^{-n}$   $n=2, 3$  and 4 .*

Optik, 114, 525-528.

**Alamir A. S. A. (2004)**

*On the chromatic aberration of magnetic lenses with a field distribution in the form of an inverse power law ( $\mathcal{B}(z) \propto z^{-n}$ ).*

Optik 115, 227-231.

**Alamir A. S. A. (2005)**

*On the optical properties of monopole, multipole, magnetic lenses.*

Optik, 116, 429-432.

**Al-Obaidi, H. N (1995)**

*Determination of the design of magnetic electron lenses operated under preassinged magnification conditions.*

Ph.D. Thesis, Baghdad University, Baghdad, Iraq.

**Berz M. (1989)**

*Differential algebraic description of beam dynamics to very high orders.*

Partical Accelerators, 24, 109-124.



**Bohumila L. (1988)**

*On the design of electron beam deflection systems.*

Optik, 79, 1-12.

**Egerton R.f. (2007)**

*Physical principles of electron microscopy an introduction to TEM, SEM, and AEM .*

(Wiley: Canada).

**Fadhil A. Ali (2006)**

*Computer – aided - design of focused ion beam for a lithography system.*

Ph.D. Thesis, Al-Nahrain University, Baghdad, Iraq.

**Goodhew, Humphreys and Beanland (2001)**

*Electron Microscopy and Analysis.*

Taylor and Francis: USA and Canada.

**Goto, E. , Soma, T., and Idesawa, M. (1978)**

*Design of a variable-aperture projection and scanning system for electron beam.*

J. Vac. Sci. Technol. 15, 883

**Goto, E. and Soma, T. (1977)**

Optik, 48, 255.

**Hajime O. (1978)**

*Moving objective lens and the Fraunhofer condition for pre-deflection.*

Optik, 53, 63-68.

**Hawkes (1982)**

*Magnetic electron Lenses.*

MSpringer-Verlag Berlin Heidelberg new York

**Hawkes P.W. (1982)**

*Magnetic Electron lenses.*

(Springer-Verlag).

**Hawkes P.W. and Kasper E. (1989)**

*Principles of electron optics vol.1.*

(Academic press: London).

**Hu K. and Tang TT (1999)**

*Lie algebra deflection aberration theory for magnetic deflection systems.*

Optik, 110, 9-14.

**Humphries, S.Jr. (1999)**

*Principle of charged particle acceleration.*

(Wiley: New York)

**Humphries, S.Jr. (2002)**

*Charged particle beams.*

(Wiley: New York).

**Jiye, X. (1981)**

*On the linear transformations for Gaussian trajectory parameters in the combined electron optical systems.*

Optik, 59, 237-249.

**Karries T. (2004)**

*Numerical Analysis Using MATLAB and Spreadsheets.*

(Wiley: New York)

**Kreyszig, E. (1983)**

*Advance engineering mathematics.*

(Wiley: Canada).

**Kuroda, K. (1980)**

*Simplified method for calculating deflective aberration of electron optical system with tow deflectors and lens.*

Optik, 57, 251-258.

**Kuroda, K., Ozasa S. and Komoda K. (1983)**

*A simplified focusing and deflection system with vertical beam landing.*

J. Vac. Sci. Technol. B1, 1303-1306.

**Lencova B. (1997)**

*Electrostatic Lenses.*

Handbook of Charged Particle Optics.

Edited by J. Orloff, 177- 222.

**Lencova B. and Wisselink G. (2001)**

*MLD (Magnetic Lens Design).*

Particle Optics Group, TU Delft and SPOC, Brno.

**Lencova, B.(1988)**

*On the design of electron beam deflection systems .*

Optik, 79, 1-12.

**Li Y., Kuangs S., Fen Z. and Liu T. (1993)**

*The relativistic fifth-order geometrical aberrations of a combined focusing-deflection system.*

J. Phys. D, Appl. Phys. 26, 522.

**Liping W., John R., Haoning L., Eric M. and Xieqing Z. (2004)**

*Simulation of electron optical systems by differential algebraic method combined with hermite fitting for practical lens fields.*

Microelectronic engineering, 73-74, 90-96.

**Marton L. (1980)**

*Advances in Electronics and Electron Physics.*

Academic press: London

**Munro E. (1974)**

*Calculation of the optical properties of combined magnetic lenses and deflection systems with superimposed field..*

Optik, 39, 450-466.

**Munro E. (1975)**

*Design and optimization of magnetic lenses and deflection systems for electron beams.*

J. Vac. Sci. Technol. 12, 1146-1151.

**Munro E. and Chu H. C. (1981b)**

*Computation of fields in magnetic deflectors.*

Optik, 60, 371-390.

**Ohiwa H. (1977)**

*Designing air core scanning systems comprising round lenses and saddle type deflection coils.*

J. Phys. D10, 1437-1449.

**Ohiwa, H. (1978)**

*Design of electron-beam scanning systems using the moving objective lens .*

J. Vac. Sci. Technol. 15, 849

**Ohiwa, H., Goto, E., and Ono, A. (1971)**

*Electron .*

Commun. Jpn., 54B, 44-51

**Philip C. (1999)**

*Introduction to electron beam lithography.*

Institute for micromanufacturing.

**Richard C. Booton Jr (1992)**

*Computational Methods for Electromagnetics and Microwaves.*

Wiley series in Microwave and optical engineering.

**Septier A. (1980)**

*Applied Charge Particle Optics part B pp.102.*

Academic press: New York, London, Toronto, Sydney, and San Francisco.

**Steven T. Karris (2004)**

*Numerical Analysis using MATLAB and Spreadsheets.*

(Prindle: United States of America).

**Szilagi, M. (1988)**

*Electron and ion optics.*

(Plenum: New York)

**Szilagyi, M. (1988)**

*Electron and ion optics.*

(Plenum: New York).

**Tahir K. (1985)**

*Critical assessment of the finite element method for calculating magnetic fields in*

*electron optics.*

Ph.D. Thesis, University of Aston, Birmingham, UK.

**Teruo H. (2002)**

*Relationship between the fifth order aberration coefficients.*

Optik, 113, 105-110.

**Tsimring S.E. (2007)**

*Electron beams and microwave vacuum electronics.*

(Wiley: Canada).

**Tsuno K. and Harada Y.(1981)**

*Elimination of spiral distortion in electron microscopy using an asymmetrical triple pole piece lens.*

(J. phys. E: Sci. Instrum. 14, 955-960).

**Uno Y., Morita H., Simazu N. and Hoskawa T. (1995)**

*Fifth-order aberration analysis of a combined electrostatic-magnetic focusing-deflection system.*

Nucl. Instrum. Method Phys. Res. A363, 10.

**Wang L. P., Tang T. T., cheng B. J. and Cleaver J. R. A. (2002)**

*Differential algebraic method for arbitrary-order aberration analysis of combined electron beam focusing-deflection systems.*

Optik, 113, 181-187.

**Wang L.B. (2002)**

*Differential algebraic method for arbitrary-order aberration analysis of combined electron beam focusing-deflection system.*

Optik 113, 181-187

**Wang L.P., Tang T.T. and Cheng B.J.(2000)**

*Differential algebraic theory and calculation for arbitrary high order aberrations of electron lenses.*

Optik, 111, 285-289.

**Yan R., Tiantong T., Yongfen K., and Xiaoli G.(2007)**

*The aberration theory of a combined electron focusing deflection system with a rotating deflection field following the rotation of the electrons.*

Optik, 118, 569-574.

**Zhuming L. and Wenqi G. (2005)**

*New method to correct eddy current in magnetic focusing-deflection system.*

Microelectronic Engineering, 78-79, 34-38.



## الخلاصة

تم إجراء بحث حاسوبي لتصميم نظام حرف وتبئير مغناطيسي باستعمال التقريب التركيبي لطريقة الأمثلية. عن طريق حل معادله الشعاع المحوري بأستخدام طريقة رنج-كوتا-نيوستروم تم إيجاد الخواص البصرية و مسار الالكترن لنظام الحرف والتبئير المغناطيسي تحت شرط التكبير الغير محدود و شرط التكبير صفري . تم استخدام التقريب التركيبي لطريقة الأمثلية في الدراسة الحالية لإيجاد التصميم الأمثل لنظام الحرف والتبئير المغناطيسي التي تعطي اقل زيوغ كروي، لوني، تشوه الحلزوني و تشوه نصف قطري.

( toroidal yoke deflection coil )تم استخدام ملف الانحراف الحلقي) مصدرا للمجال المغناطيسي، وكذلك توزيع المجالتم تحديده باستخدام الدالة الأسية. فكرة العدسة الشبئية المتحركة اعتمدت في حساب مجال النظام. زيوغ النظام خفض بتغيير الشكل الهندسي لملف الانحراف، حيث غير الطول والزاوية.

باستخدام أمثل توزيع للمجال المحوري تم إيجاد شكل قطع القطب التي تعطي توزيع المجال هذه باستخدام طريقة أعاده البناء.

بينت الحسابات بأن اقل معاملات الزيوغ تظهر عندما يكون طول الملف

$$(H=23\text{mm}) (\theta=61^\circ)$$

إن العلاقة عكسية بين المعاملات الأربعة والطول و الزاوية في حالتني شرط التكبير الصفري  
والغير محدد وعلية فأنة يوفر لنا أمكانية تشغيل المنظومة بكفاءة عالية في مختلف شروط تشغيل  
المنظومة.



جمهورية العراق  
وزارة التعليم العالي و البحث العلمي  
جامعة النهرين  
كلية العلوم

# حسابات الأمثلية لمنظومة مغناطيسية

تأليف من حارفة و محذسه

رسالة

مقدمة إلى كلية العلوم في جامعة النهرين وهي جزء من متطلبات نيل  
درجة الماجستير في علوم الفيزياء

من قبل

**احمد حسين علي**

(بكالوريوس ٢٠٠٦)

باشرافه

الأستاذ المساعد الدكتور احمد جمال احمد و الدكتور محدي علي حسين

في

كانون الأول ٢٠٠٨م

ذي الحجة ١٤٢٩هـ

